HSP40 proteins use class-specific regulation to drive HSP70 functional diversity

Hsp40s employ class-specific regulation to drive Hsp70 functional diversity

Ofrah Faust[1,5], Meital Abayev-Avraham[1,5], Anne S. Wentink[2], Michael Maurer[1,2], Nadinath B. Nillegoda[2,3], Nir London[4], Bernd Bukau[2,*] and Rina Rosenzweig[1,*]

[1]Department of Structural Biology, Weizmann Institute of Science, Rehovot, 761000, Israel.

[2]Center for Molecular Biology of Heidelberg University (ZMBH) and German Cancer Research Center (DKFZ), DKFZ-ZMBH Alliance, Im Neuenheimer Feld 282, 69120, Heidelberg, Germany.

[3]Australian Regenerative Medicine Institute (ARMI), Monash University, Clayton, VIC, Australia.

[4]Department of Organic Chemistry, Weizmann Institute of Science, Rehovot, 761000, Israel.

[5]These authors contributed equally: Ofrah Faust and Meital Abayev-Avraham.

[*]rina.rosenzweig@weizmann.ac.il

[*]bukau@zmbh.uni-heidelberg.de

Abstract

The ubiquitous heat shock protein 70 (Hsp70) family are ATP-dependent molecular chaperones that perform a myriad of cellular functions, affecting virtually all aspects in the life of proteins from synthesis to degradation[1-3]. Achieving this broad spectrum of functions requires precise regulation of Hsp70 activity. Hsp40s, also known as J-domain proteins (JDPs), play a key role in this crucial process by pre-selecting substrates for transfer to their Hsp70 partners and stimulating Hsp70 ATP hydrolysis, leading to stable substrate binding[3,4]. In humans, JDPs constitute a large and diverse family with over 40 different members[2], which vary in their substrate selectivity and the nature and number of their client binding domains[5]. Here we show that JDPs can also differ fundamentally in their interaction with Hsp70 chaperones. Using nuclear magnetic resonance spectroscopy[6,7] we find that the major class B JDPs are regulated by a novel autoinhibitory mechanism not present in other classes. While in all JDPs the interaction of the characteristic J-domain (JD) is responsible for activation of Hsp70, in DnaJB1 the Hsp70-binding sites in this domain are intrinsically blocked by the adjacent GF-rich region - an inhibition which can be lifted upon interaction of a second site on DnaJB1 with the Hsp70 C-terminal tail. This regulation, which controls substrate targeting to Hsp70, is essential for disaggregation of amyloid fibers by Hsp70-DnaJB1, shedding light on why no other class of JDPs can substitute for class B in this critical function. Moreover, this previously undiscovered regulatory layer governing the functional specificities of JDP co-chaperones and their interactions with Hsp70s may be key to the expansive gamut of Hsp70 functions in the cell.

Main

JDPs are multidomain proteins, characterized by the conserved signature J-domain (JD)[2], that binds to the interface between the Hsp70 nucleotide binding domain (NBD) and substrate binding domain (SBD), and is required for stimulation of Hsp70 ATPase activity[8]. Canonical class A and B JDPs also comprise a glycine-rich (GF) region adjacent to the N-terminal J-domain, two structurally similar C-terminal β-barrel domains (CTDI and CTDII) containing the substrate binding region, and a dimerization domain[2]. Class A JDPs further contain a zinc-finger-like region (ZFLR) protruding from CTDI (Fig. 1a).

JDPs are an intriguing example of proteins from the same family which, while structurally very similar, confer distinct activities in the cell, with this functional diversity generally thought to arise from differences in targeting of Hsp70 chaperones to substrates[9-11]. It is therefore quite puzzling that, while both classes A and B display similar affinity for amyloid fibers, such as α-synuclein and Tau, only class B JDPs have the ability to harness Hsp70 to perform efficient fiber disaggregation[12-16]. The causes of this diverging behavior, however, and hence the molecular basis of Hsp70 activation for chaperone action on selective substrates, have thus far remained elusive.

Class A and B JDP interaction with Hsp70

To investigate the reasons behind the functional divergence between class A and class B JDPs, we first used solution NMR to compare the interaction of Hsp70 with the isolated J-domains of human DnaJA2 and DnaJB1, as these domains are known to both bind and activate the Hsp70 chaperone[2]. In both cases, we observed selective peak broadening for J-domain residues localized at the end of helix II and the conserved HPD motif (residues 31-41 in DnaJA2 and 28-37 in DnaJB1), and in helix III (residues 47-53 in DnaJA2 and 46-51 in DnaJB1) (Fig. 1b-d; Extended Data Fig. 1a,b) - indicating the proximity of these residues to the Hsp70 chaperone (i.e. binding). Both interactions also closely resembled that of the bacterial JDP, DnaJ, with its partner Hsp70, DnaK[8], demonstrating the highly conserved nature of JD-Hsp70 binding.

Given the minor differences in the JD-driven binding of the two co-chaperones to Hsp70, we next probed the importance of the disordered GF-rich linker, as this domain was reported to be essential in bacteria for maximal stimulation of DnaK (Hsp70) ATPase activity[17,18,19].

The NMR spectrum of DnaJA2^{JD-GF} (residues 1-111) containing both the JD and GF regions was very similar to that of isolated J-domain, with additional peaks appearing in the random coil regions that corresponded to the GF-rich linker (Fig. 1e). Upon addition of Hsp70, DnaJA2^{JD-GF} J-domain residues showed the same selective peak broadening as observed for Hsp70 binding to the isolated JD (Fig 1b). The GF-rich linker residues,

however, were largely unaffected (Fig. 1c), suggesting that this linker does not participate directly in the interaction with Hsp70. Similar results were obtained for the more abundant class A JDP, DnaJA1 (Extended Data Fig. 1c,d).

The class B JDP, DnaJB1, however, displayed decidedly different behavior, with no binding whatsoever being detected between Hsp70 and DnaJB1$^{JD\text{-}GF}$ (res 1-111), even upon addition of excess protonated Hsp70 (Fig. 1f). This was surprising, as addition of the same concentration of protonated Hsp70 to the isolated J-domain (without the GF region) caused very significant peak broadening (Extended Data Fig. 1e).

DnaJB1 GF region inhibits JD-Hsp70 binding

In addition to the lack of interaction with Hsp70, the DnaJB1$^{JD\text{-}GF}$ construct itself also displayed a different pattern of chemical shifts compared to the J-domain alone, with the largest changes being observed in helix II and III of the JD, corresponding to the Hsp70 binding region, and helix IV (Extended Data Fig. 1f). Further analysis of DnaJB1$^{JD\text{-}GF}$ NMR chemical shifts using TALOS+ [20] (Extended Data Fig. 2a) and $^{1}D_{NH}$ residual dipolar coupling (RDC) measurements[21] (Extended Data Fig. 2b), revealed a stable alpha helix that forms between residues 98-106, a region previously suggested to be disordered. Measurement of the local backbone flexibility in the ns-ps time-scale further indicated that residues 93-107 in the GF region are highly structured, with calculated order parameters of 0.9-1.0 (see Methods, Extended Data Fig. 2c).

We then determined the structure of DnaJB1$^{JD\text{-}GF}$ using solution NMR (Extended Data Fig. 2c-h and Supplementary Table 1). This showed that, while DnaJB1$^{JD\text{-}GF}$ residues 1-71 adopt a similar fold to that of the isolated J-domain[22], helix V docks onto helix II and III of the J-domain, covering the Hsp70 binding sites (Fig. 1g).

To determine whether this newly identified helix V is what is responsible for blocking the interaction with Hsp70, we generated an additional truncation mutant in which the entire helix was deleted (DnaJB1$^{1\text{-}96}$). DnaJB1$^{1\text{-}96}$ displayed a strong restored interaction with

Hsp70 and showed similar chemical shift patterns to that of the isolated JD, with differences observed only in helix IV (Extended Data Fig. 3a,b).

We next tested whether the inhibiting helix also exists in the context of full-length DnaJB1. Indeed, careful comparison of the chemical shifts from the ILVM-labelled methyl-TROSY spectra of full-length DnaJB1, DnaJB1$^{JD\text{-}GF}$ and DnaJB1^{JD} revealed that the full-length DnaJB1 adopts the same JD-inhibited conformation as DnaJB1$^{JD\text{-}GF}$ (Extended Data Fig. 3c). This then poses the question of how this inhibition is lifted to allow Hsp70 binding, as DnaJB1 has long been known to both bind and activate Hsp70. We therefore set out to determine the mechanism through which this intramolecular inhibition is released in the full-length DnaJB1 co-chaperone.

DnaJB1 contains a second Hsp70 binding site

We began by monitoring the chemical shift changes of full length DnaJB1 upon addition of Hsp70. In line with previous observations, addition of Hsp70 to DnaJB1 resulted in chemical shift perturbations (Fig. 2a and Extended Data Fig. 4) and selective peak broadening (Fig. 2b), indicating binding and confirming that, in the context of the full-length protein, the GF inhibition of the Hsp70 binding site on the J-domain is lifted. Assignment of DnaJB1 revealed that Hsp70, in fact, binds to two distinct sites on the co-chaperone – one located at the J-domain, and another in CTDI (Fig. 2b,c), with subsequent NMR experiments further revealing that the Hsp70-CTDI interaction can occur independently of binding to J-domain (Extended Data Fig. 4b,c). As the isolated CTDI from both DnaJB1 and its yeast homolog Sis1 was previously shown to interact with a conserved EEVD tetrapeptide from the C-termini of eukaryotic cytosolic Hsp70s[23-25], we asked whether this EEVD tail acts as the additional DnaJB1-binding site on Hsp70 chaperones.

To test this hypothesis, we repeated the NMR binding experiment, this time using methyl-labeled Hsp70 and titrating in deuterated DnaJB1 (Extended Data Fig. 5a). The same NMR experiments were also performed with isolated DnaJB1 J-domain and CTDI, as the J-domain and CTDI DnaJB1 regions can interact independently with Hsp70 (Extended Data

Fig. 5b,c). As expected, the J-domain of DnaJB1 bound to the interface between the Hsp70 SBD and NBD, similarly to the contacts between DnaK and DnaJ JD[8]. DnaJB1 CTDI was indeed found to interact with the C-terminal tail of Hsp70, with this interaction occurring both for full-length DnaJB1 (Fig. 2d) and a construct containing only the CTDs.

In yeast Hsp70 (Ssa1), the presence of the C-terminal EEVD tail is essential for proper protein folding by the combined activity of Hsp70 and class B JDP Sis1, although, interestingly, not for the same activity when performed by Hsp70 and class A JDPs such as Ydj1[23,26]. We were therefore curious whether and how the interaction between the Hsp70 EEVD tail and the CTDI differs between these class A and B JDPs. To investigate this, we repeated the Hsp70 binding experiment using the class A JDP, DnaJA2. Like DnaJB1, DnaJA2 showed strong interaction with Hsp70 through its J-domain, however, no binding was detected between the CTDs of DnaJA2 and the Hsp70 C-terminal EEVD region (Fig. 2d, Extended Data Fig. 5c-d). Therefore, there is a striking difference between the highly homologous class A and B JDPs in their mode of binding to Hsp70s. Class B co-chaperones demonstrate both intrinsic inhibition of their J-domain and an additional Hsp70 binding site, while class A JDPs have neither.

EEVD binding to DnaJB1 releases JD-GF inhibition

Next, we wanted to determine whether the interaction of DnaJB1 CTDI with the C-terminal EEVD tail of Hsp70 correlates with the release of the GF inhibition of the J-domain. To test this, we generated a peptide corresponding to the last 20 amino acids of the Hsp70 EEVD. Titration of this peptide into methyl labeled DnaJB1 resulted in chemical shift perturbations (CSPs) at the same CTDI residues that were found in our NMR experiments to interact with full-length Hsp70 (compare Extended Data Fig. 4a,d), indicating that Hsp70 interacts with the DnaJB1 CTDs solely through its C-terminal disordered region. In addition, the binding affinity of the peptide was rather weak (k_D=50±7µM), suggesting that this interaction is transient in nature. Importantly, though, the addition of the peptide also resulted in changes to the resonances of the DnaJB1 J-domain (Fig. 3a, indicated by an asterisk). There, residues in helix II and III exhibited changes in the slow time scale -

corresponding to a reduction in the intensity of the GF-inhibited JD conformation and a buildup of the released-JD state (Fig. 3b).

We next used paramagnetic relaxation enhancement (PRE) experiments[27,28] to determine the proximity of the Hsp70-EEVD-binding site on DnaJB1 CTDI to the J-domain GF-complex, where the release occurs. This was performed using nitroxide spin-probes attached either to residue 40 in helix III of the J-domain, or residue 186 in CTDI. Significant decreases in peak intensities were observed in the CTDI region upon spin labeling of J-domain and in JD-GF upon CTDI labeling (Fig. 3c,d, dark-blue bars), indicating that in DnaJB1, the J-domain is positioned within 12-17Å of CTDI. Addition of the EEVD-containing peptide, however, completely abolished the intensity decrease in these regions (Fig. 3c,d, purple bars), revealing that upon peptide binding, the J-domain detaches from CTDI, moving beyond the sensitive range of the PRE experiments (>30Å).

We similarly attached spin labels to residues at the two ends of GF inhibitory-helix V (residues 93 and 108) and recorded the PREs. These measurements show that upon Hsp70 interaction, helix V also detaches from CTDI as well as from the J-domain (Fig. 3e,f). Therefore, the direct interaction of DnaJB1 CTDI with the Hsp70 EEVD tail releases the GF inhibition of the DnaJB1 JD, freeing it for subsequent Hsp70 binding and activation.

DnaJB1 binds Hsp70 / substrates independently

The DnaJB1 CTDI region that interacts with the Hsp70 EEVD tail was also previously proposed to serve as a binding site for peptides and unfolded client proteins[5,29]. This, then, alluded to the possibility that the Hsp70 EEVD mimics substrates in its binding. We therefore tested whether the Hsp70 C-terminal tail competes with client proteins for DnaJB1 binding, and whether substrates are also capable of releasing the GF inhibition of DnaJB1 J-domain.

Titrating a known substrate, α-synuclein[12], to DnaJB1 showed binding primarily in CTDII, separate from the CTDI site for the Hsp70 EEVD, with no changes being observed for J-domain residues (Extended Data Fig. 6a). Thus the release of DnaJB1 JD-GF inhibition,

and subsequent Hsp70-DnaJB1 binding and activation, is solely dependent on the interaction of the C-terminal Hsp70 tail with CTDI.

Furthermore, competition experiments with either addition of EEVD peptide to DnaJB1-substrate complex, or α-synuclein to DnaJB1-EEVD peptide, showed that substrates and Hsp70 C-terminal peptide can simultaneously bind to DnaJB1 (Extended Data Fig. 6c-d).

EEVD deletion abolishes Hsp70-DnaJB1 binding

We next tested the effect of the deletion of the last four Hsp70 residues, corresponding to the conserved EEVD sequence. This deletion completely abolished the DnaJB1-Hsp70 interaction (Fig. 3g), yet had no effect on Hsp70 interaction with DnaJA2 (Extended Data Fig. 7), reinforcing the conclusion that class A co-chaperones bind to Hsp70 solely through their J-domain (Extended Data Fig. 7). Interaction of CTDI with the Hsp70 C-terminal tail is thus an essential step exclusively for class B JDP binding and activation of Hsp70. The inability of mutated Hsp70 to interact with DnaJB1 also explains the previous observation that $Hsp70^{\Delta EEVD}$ is defective in protein refolding with class B JDPs, but not with class A co-chaperones[23,26], which neither possess the interaction site for Hsp70 EEVD, nor the intrinsic JD inhibition which this binding is required to abate.

We thus find that the two JDP classes, despite their high structure and sequence similarities, interact and activate the Hsp70 chaperone in different manners. Class A JDPs, such as DnaJA2 and DnaJA1, only interact with Hsp70 via their N-terminal J-domains. Class B JDP, DnaJB1, however, displays a more complex two-step Hsp70-binding behavior introduced by the existence of a structured helix (V) within the GF region. This helix, which is not found in class A JDPs, is initially docked onto the DnaJB1 J-domain, preventing it from interacting with Hsp70. It is only upon interaction of the DnaJB1 CTDI with the C-terminal tail of Hsp70, that the J-domain is released, allowing it to bind and activate the Hsp70 chaperone (Fig. 4a).

GF mutations restore DnaJB1-Hsp70$^{\Delta EEVD}$ function

To understand the importance of the two-step binding mechanism in DnaJB1, we generated mutations designed to disrupt the JD-GF interface - E50A (DnaJB1^{E50A}) and F102A (DnaJB1^{F102A}) (Extended Data Fig. 8a). The DnaJB1^{JD-GF} constructs of both mutants exhibited an NMR spectra indicative of two slowly exchanging conformations, one corresponding to the GF-inhibited and one to the free J-domain state (Extended Data 8d,e). Moreover, unlike the previously shown wild-type DnaJB1^{JD-GF} construct, that displayed no binding to Hsp70 (Extended Data Fig. 8b,c vs Fig. 1b), both mutants showed strong binding to the chaperone, further proving that release of JD inhibition is strictly required for DnaJB1^{JD}-Hsp70 interaction. In addition, while DnaJB1^{WT} was unable to interact with Hsp70$^{\Delta EEVD}$, the mutants, which are no longer dependent on interaction with the EEVD tail to release the J-domain, showed tight binding to the chaperone (Extended Data Fig. 9 a-c). This lack of reliance on the CTDI-Hsp70-EEVD interaction also explains previous observations that the E50A mutant can partially rescue the refolding activity of Hsp70$^{\Delta EEVD}$ [23,26]. As expected, while addition of Hsp70^{WT} to methyl-labeled DnaJB1 resulted in perturbations to both the JD and CTDI regions of DnaJB1 (Extended Data Fig. 9d-f), Hsp70$^{\Delta EEVD}$ only bound to the J-domain - again confirming that the EEVD region is the sole point of interaction for DnaJB1 CTDI.

The two DnaJB1 mutants could, however, only partially restore the refolding of denatured luciferase activity of Hsp70$^{\Delta EEVD}$, while refolding by Hsp70^{WT} was as efficient with the mutants as with DnaJB1^{WT} (Fig. 4c). This reduced refolding activity of the mutants may be due to lower affinity for Hsp70$^{\Delta EEVD}$ resulting from the lack of the CTDI-Hsp70 interaction (Extended Data Fig. 9), to the only partially-released state of the JD (64% in E50A and 36% in F102A) (Extended Data Fig. 8d,e), or a combination of both.

To discriminate between these possibilities, we designed a DnaJB1 construct containing five mutations in helix V (H99G, M101S, F102G, F105S, and F106G), producing high resemblance to the unstructured DnaJA2 GF sequence. This DnaJB1$^{\Delta H5}$ mutant, which had a perpetually released J-domain (Extended Data Fig. 10a,b), bound Hsp70$^{\Delta EEVD}$ with high affinity, and fully enhanced Hsp70 ATPase rates at sub-stoichiometric concentrations

(Extended Data Fig. 10c,d). Like the previous two mutants, DnaJB1$^{\Delta H5}$, in conjunction with full-length Hsp70, refolded denatured firefly luciferase as efficiently as DnaJB1^{WT} (Fig. 4c), and in fact achieved higher substrate refolding rates - explaining why class A JDPs, that lack the autoinhibition observed in DnaJB1, are more efficient in the refolding of misfolded substrates than class B JDPs. Unlike the partially released mutants, however, DnaJB1$^{\Delta H5}$ also retained this same level of activity with Hsp70$^{\Delta EEVD}$ (Fig. 4c), indicating the interaction of the Hsp70 C-terminal tail with DnaJB1 CTDI does not play a role in protein refolding beyond the release of the GF inhibition of the J-domain.

JD-GF inhibition is essential for amyloid disaggregation

It thus appears that the J-domain autoinhibition and release mechanism in DnaJB1 does not offer any functional advantage in protein folding over class A JDPs, which have an intrinsically free J-domain. We therefore set out to test whether this regulation may instead play an essential role in the disaggregation of amyloid fibrils, where class A JDPs are unable to substitute for their class B paralogs[12,13,15,16].

To this end, we tested the function of DnaJB^{E50A}, DnaJB1^{F102A}, and DnaJB1$^{\Delta H5}$ mutants in protein disaggregation. DnaJB1^{WT}, together with Hsp70 and the nucleotide exchange factor (NEF) Hsp110, successfully disaggregated 85% of preformed α-synuclein fibers, while under the same conditions DnaJB1^{E50A} and DnaJB1^{F102A} mutants showed reduced disaggregation rates (70% and 47%, respectively). Unlike the DnaJB1^{WT}, however, both mutants could still partially disaggregate α-synuclein fibers together with Hsp70$^{\Delta EEVD}$ (Fig. 4d). In contrast, DnaJB1$^{\Delta H5}$, which has a fully released J-domain was unable to promote the disaggregation of α-synuclein fibers with either Hsp70^{WT} or Hsp70$^{\Delta EEVD}$. This mutant, though, both binds to the fibers with similar affinity as DnaJB1^{WT} (Extended Data Fig. 10e), and interacts strongly with Hsp70 (Extended Data Fig. 10f) recruiting it to the fibers (Extended Data Fig. 10g, h). These assays therefore strongly indicate that the autoinhibition of the DnaJB1 J-domain, and its release through the CTDI interaction with the Hsp70 terminal tail, are essential for protein disaggregation, as even a partial release of the inhibition reduces disaggregation activity.

A parallel study (Wentink et al, 2020) identified that recruitment of Hsp70 molecules, at high density, to α-synuclein fibrils is key to efficient amyloid disaggregation. We thus tested whether the ability of JDPs to cluster Hsp70 chaperones is likewise dependent on the autoinhibitory mechanism. Proximity of Hsp70 chaperones on a fibril surface was measured using fluorescence resonance energy transfer (FRET) experiments in the presence of DnaJB1, DnaJA2, or the mutant DnaJB1$^{\Delta H5}$, which has a functional Hsp70 binding site on CTDI, but does not contain the autoinhibitory helix-V. Interestingly, the assay showed that only the combination of DnaJB1^{WT} and Hsp70^{WT} fostered efficient clustering (Extended Data Fig. 10i), demonstrating that both the GF inhibition of the J-domain and its docking onto the CTD are vital for efficient targeting and clustering of Hsp70 onto the amyloid fibers.

We next asked if artificially improving Hsp70 clustering around the reduced-efficacy DnaJB1 mutants could restore their disaggregation activity. We thus repeated the disaggregation assays with an excess of Hsp110, as Wentink et al. showed that Hsp110 displays a biased NEF activity towards Hsp70 molecules that are not densely packed onto the fibrils - thereby actively increasing the proportion of efficiently clustered Hsp70 molecules (Wentink et al, 2020). Addition of increasing concentrations of Hsp110 NEF indeed partially rescued the disaggregation function of the DnaJB1$^{\Delta H5}$ mutant (Fig. 4e), but had no such effect on DnaJA2.

These experiments therefore establish why class A JDPs, which have similar affinity for α-synuclein fibers as DnaJB1 (Extended Data Fig. 10e), but do not possess a similar autoinhibitory mechanism, are incapable of participating in amyloid disaggregation[12].

Overall, our results show that the DnaJB1 chaperone has evolved a regulatory mechanism for precise control of the critical Hsp70 targeting step to client proteins, which is both unique and vital to its functions. Moreover, as the inhibitory helix-V region is also highly conserved across class B JDPs, such regulation most likely governs the activity of all cytosolic members of this family, with perhaps the prime example being DnaJB6[30], where mutations in this region result in distal myopathy disorders[31]. Interestingly, of the class B

family there are only two members that do not contain the helix-V region - the ER-localized DnaJB9 and DnaJB11. These, however, are known to be co-chaperones for HSPA5 (Bip)[32], which does not contain the corresponding EEVD tetrapeptide at its C-terminus required to release the JD-GF inhibition.

It therefore seems that we have just begun to scratch the surface in understanding this newly identified layer of regulation, and its importance in the many functions of class B chaperones in the cell.

References

1 Mayer, M. P. & Bukau, B. Hsp70 chaperones: cellular functions and molecular mechanism. *Cell Mol Life Sci* **62**, 670-684, doi:10.1007/s00018-004-4464-6 (2005).

2 Kampinga, H. H. & Craig, E. A. The HSP70 chaperone machinery: J proteins as drivers of functional specificity. *Nat Rev Mol Cell Biol* **11**, 579-592, doi:10.1038/nrm2941 (2010).

3 Rosenzweig, R., Nillegoda, N. B., Mayer, M. P. & Bukau, B. The Hsp70 chaperone network. *Nat Rev Mol Cell Biol*, doi:10.1038/s41580-019-0133-3 (2019).

4 Tiwari, S., Kumar, V., Jayaraj, G. G., Maiti, S. & Mapa, K. Unique structural modulation of a non-native substrate by cochaperone DnaJ. *Biochemistry* **52**, 1011-1018, doi:10.1021/bi301543g (2013).

5 Jiang, Y., Rossi, P. & Kalodimos, C. G. Structural basis for client recognition and activity of Hsp40 chaperones. *Science* **365**, 1313-1319, doi:10.1126/science.aax1280 (2019).

6 Tugarinov, V., Hwang, P. M., Ollerenshaw, J. E. & Kay, L. E. Cross-correlated relaxation enhanced 1H[bond]13C NMR spectroscopy of methyl groups in very high molecular weight proteins and protein complexes. *J Am Chem Soc* **125**, 10420-10428, doi:10.1021/ja030153x (2003).

7 Tugarinov, V., Kanelis, V. & Kay, L. E. Isotope labeling strategies for the study of high-molecular-weight proteins by solution NMR spectroscopy. *Nat Protoc* **1**, 749-754, doi:nprot.2006.101 [pii] 10.1038/nprot.2006.101 (2006).

8 Kityk, R., Kopp, J. & Mayer, M. P. Molecular Mechanism of J-Domain-Triggered ATP Hydrolysis by Hsp70 Chaperones. *Mol Cell* **69**, 227-237 e224, doi:10.1016/j.molcel.2017.12.003 (2018).

9 Wentink, A., Nussbaum-Krammer, C. & Bukau, B. Modulation of Amyloid States by Molecular Chaperones. *Cold Spring Harb Perspect Biol* **11**, doi:10.1101/cshperspect.a033969 (2019).

10 Schilke, B. A. *et al.* Broadening the functionality of a J-protein/Hsp70 molecular chaperone system. *PLoS Genet* **13**, e1007084, doi:10.1371/journal.pgen.1007084 (2017).

11 Zarouchlioti, C., Parfitt, D. A., Li, W., Gittings, L. M. & Cheetham, M. E. DNAJ Proteins in neurodegeneration: essential and protective factors. *Philos Trans R Soc Lond B Biol Sci* **373**, doi:10.1098/rstb.2016.0534 (2018).

12 Gao, X. *et al.* Human Hsp70 Disaggregase Reverses Parkinson's-Linked alpha-Synuclein Amyloid Fibrils. *Mol Cell*, doi:10.1016/j.molcel.2015.07.012 (2015).

13 Rampelt, H. *et al.* Metazoan Hsp70 machines use Hsp110 to power protein disaggregation. *EMBO J* **31**, 4221-4235, doi:10.1038/emboj.2012.264 (2012).

14 Duennwald, M. L., Echeverria, A. & Shorter, J. Small heat shock proteins potentiate amyloid dissolution by protein disaggregases from yeast and humans. *PLoS Biol* **10**, e1001346, doi:10.1371/journal.pbio.1001346 (2012).

15 Scior, A. *et al.* Complete suppression of Htt fibrilization and disaggregation of Htt fibrils by a trimeric chaperone complex. *EMBO J* **37**, 282-299, doi:10.15252/embj.201797212 (2018).

16 Nachman E., W. A., Madiona K., Bousset L., Katsinelos T., Kampinga H., McEwan WA., R. Jahn RT., Melki R., Mogk A., Bukau B., and Nussbaum-Krammer C. Disassembly of Tau fibrils by the human Hsp70 disaggregationmachinery generates small seeding-competent species *bioRxiv*, doi:http://dx.doi.org/10.1101/2019.12.16.876888 (2019).

17 Minami, Y., Hohfeld, J., Ohtsuka, K. & Hartl, F. U. Regulation of the heat-shock protein 70 reaction cycle by the mammalian DnaJ homolog, Hsp40. *J Biol Chem* **271**, 19617-19624, doi:10.1074/jbc.271.32.19617 (1996).

18 Karzai, A. W. & McMacken, R. A bipartite signaling mechanism involved in DnaJ-mediated activation of the Escherichia coli DnaK protein. *J Biol Chem* **271**, 11236-11246 (1996).

19 Yan, W. & Craig, E. A. The glycine-phenylalanine-rich region determines the specificity of the yeast Hsp40 Sis1. *Mol Cell Biol* **19**, 7751-7758 (1999).
20 Shen, Y. & Bax, A. Protein backbone and sidechain torsion angles predicted from NMR chemical shifts using artificial neural networks. *J Biomol NMR* **56**, 227-241, doi:10.1007/s10858-013-9741-y (2013).
21 Mesleh, M. F., Veglia, G., DeSilva, T. M., Marassi, F. M. & Opella, S. J. Dipolar waves as NMR maps of protein structure. *J Am Chem Soc* **124**, 4206-4207, doi:10.1021/ja0178665 (2002).
22 Qian, Y. Q., Patel, D., Hartl, F. U. & McColl, D. J. Nuclear magnetic resonance solution structure of the human Hsp40 (HDJ-1) J-domain. *J Mol Biol* **260**, 224-235, doi:10.1006/jmbi.1996.0394 (1996).
23 Yu, H. Y. *et al.* Roles of intramolecular and intermolecular interactions in functional regulation of the Hsp70 J-protein co-chaperone Sis1. *J Mol Biol* **427**, 1632-1643, doi:10.1016/j.jmb.2015.02.007 (2015).
24 Li, J., Wu, Y., Qian, X. & Sha, B. Crystal structure of yeast Sis1 peptide-binding fragment and Hsp70 Ssa1 C-terminal complex. *Biochem J* **398**, 353-360, doi:10.1042/BJ20060618 (2006).
25 Craig, E. A. & Marszalek, J. How Do J-Proteins Get Hsp70 to Do So Many Different Things? *Trends Biochem Sci* **42**, 355-368, doi:10.1016/j.tibs.2017.02.007 (2017).
26 Yu, H. Y., Ziegelhoffer, T. & Craig, E. A. Functionality of Class A and Class B J-protein co-chaperones with Hsp70. *FEBS Lett* **589**, 2825-2830, doi:10.1016/j.febslet.2015.07.040 (2015).
27 Battiste, J. L. & Wagner, G. Utilization of site-directed spin labeling and high-resolution heteronuclear nuclear magnetic resonance for global fold determination of large proteins with limited nuclear overhauser effect data. *Biochemistry* **39**, 5355-5365, doi:bi000060h [pii] (2000).
28 Clore, G. M. & Iwahara, J. Theory, practice, and applications of paramagnetic relaxation enhancement for the characterization of transient low-population states of biological macromolecules and their complexes. *Chem Rev* **109**, 4108-4139, doi:10.1021/cr900033p (2009).
29 Suzuki, H. *et al.* Peptide-binding sites as revealed by the crystal structures of the human Hsp40 Hdj1 C-terminal domain in complex with the octapeptide from human Hsp70. *Biochemistry* **49**, 8577-8584, doi:10.1021/bi100876n (2010).
30 Karamanos, T. K., Tugarinov, V. & Clore, G. M. Unraveling the structure and dynamics of the human DNAJB6b chaperone by NMR reveals insights into Hsp40-mediated proteostasis. *Proc Natl Acad Sci U S A* **116**, 21529-21538, doi:10.1073/pnas.1914999116 (2019).
31 Ruggieri, A. *et al.* Complete loss of the DNAJB6 G/F domain and novel missense mutations cause distal-onset DNAJB6 myopathy. *Acta neuropathologica communications* **3**, 44, doi:10.1186/s40478-015-0224-0 (2015).
32 Shen, Y. & Hendershot, L. M. ERdj3, a stress-inducible endoplasmic reticulum DnaJ homologue, serves as a cofactor for BiP's interactions with unfolded substrates. *Mol Biol Cell* **16**, 40-50, doi:10.1091/mbc.e04-05-0434 (2005).

Figure legends:

Figure 1: In class B JDPs, the GF region initially blocks JD binding to Hsp70

(a) Domain organization of class A and B JDPs, with boundaries indicated underneath: J-domain (red), with enlarged secondary structure arrangement below, GF (grey), CTDI (cyan) CTDII (blue), dimerization domain (yellow), and ZFLR insertion into CTDI, only present in class A JDPs (pink). **(b-c)** $^{1}H–^{15}N$ HSQC spectra of 0.2mM DnaJA2^{JD} **(b)** and DnaJB1^{JD} **(c)** alone (black), and in complex with 0.2mM ^{2}H Hsp70 chaperone (colored). Peaks missing from the colored spectra indicate proximity to Hsp70 (binding). **(d)** Structure of DnaJB1^{JD} [22] with the Hsp70-binding region, identified by NMR in panel c, colored red. **(e)** $^{1}H–^{15}N$ HSQC spectra of 0.2mM DnaJA2^{JD-GF} alone (black), and in complex with 0.2mM ^{2}H Hsp70. While J-domain peaks of DnaJA2^{JD-GF} are similarly affected by Hsp70 interaction as in (b), peaks from the GF region are unchanged, indicating that DnaJA2 GF does not bind Hsp70. **(f)** $^{1}H–^{15}N$ HSQC spectra of 0.2mM DnaJB1^{JD-GF} alone (black), and in the presence of 0.4mM ^{1}H Hsp70 (red). No changes were observed in the spectra of DnaJB1^{JD-GF} upon addition of Hsp70, indicating lack of interaction. **(g)** Cartoon representation of 10 lowest energy solution NMR structures of DnaJB1^{JD-GF}, with helix V colored orange. Helix V docking onto the interface between HII and HIII blocks the Hsp70-binding sites on the DnaJB1 J-domain.

Figure 2: DnaJB1 contains an additional Hsp70-binding site not found in Class A chaperones

(a) Chemical shift perturbations upon titration of increasing concentrations of Hsp70 (dark to light red) into 0.2mM $^{13}CH_3$-ILVM labeled DnaJB1. **(b)** Methyl group peak intensity ratios of Hsp70-bound DnaJB1, calculated using the final concentration of the titration versus free DnaJB1 (I^{bound}/I^{free}). Significant reductions in intensity indicate Hsp70 binds to two sites on DnaJB1 - one in the J-domain and one in CTDI. **(c)** Structure of DnaJB1 CTDs (PDB ID 3AGX)[29] with significant average intensity ratio changes (greater than two standard deviations, > 0.1) colored red. **(d)** Interaction of $^{13}CH_3$-ILVM labeled Hsp70 with DnaJB1 (red, top-left), DnaJB1 JD (dark red, top-center), DnaJB1 CTDs (turquoise, top-right), DnaJA2 (blue, bottom-left), DnaJA2 JD (dark blue, bottom-center), and DnaJA2 CTDs (green, bottom-right). All experiments were measured with 0.2mM of Hsp70 and 2-fold excess of the indicated binding partner. J-domains of both DnaJB1 and DnaJA2 bind to the interface between Hsp70 NBD and SBD (see Extended Data Fig. 5 for more details). Only DnaJB1 CTDI (residue V645) interacts with the Hsp70 C-terminal EEVD tail, with no interaction observed between DnaJA2 CTDs and Hsp70.

Figure 3: DnaJB1 binding to the Hsp70 C-terminal EEVD tail releases the JD-GF inhibition

(a) Titration of 20 aa-long Hsp70 C-terminal peptide into $^{13}CH_3$-ILVM labeled DnaJB1, showing perturbations on the fast time exchange time scale to CTDI residues (marked by black arrows), and changes on the slow time scale to the J-domain residues (marked by asterisks). **(b)** Addition of Hsp70 EEVD-peptide released the GF inhibition of DnaJB1 J-domain, with residues L55, I20, and V54 displaying different chemical shifts in the GF-inhibited, docked (gray) and free JD (black) conformations. In DnaJB1, the J-domain is in a fully inhibited conformation (blue) which is partially released to the free JD state (purple) upon addition of Hsp70 C-terminal peptide. **(c-f)** Methyl group peak intensity ratios, of paramagnetic (oxidized) and diamagnetic (reduced) spin-labeled DnaJB1 at positions 40 **(c)**, 186 **(d)**, 93 **(e)**, and 108 **(f)** in the absence (blue) and presence (pink) of Hsp70 C-terminal tail (location of spin label indicated by red ellipse). In the absence of Hsp70, DnaJB1 J-domain is in close proximity to CTDI, as indicated by significant decreases in peak intensities in CTDI upon spin labeling of J-domain (c), and in the JD-GF upon labeling of CTDI (d). Addition of Hsp70 C-terminal EEVD-containing peptide abolished the intensity decrease in these regions, indicating detachment of the J-domain from CTDI. Similarly, upon Hsp70 EEVD binding, DnaJB1 GF detaches both from the J-domain and CTDI (e-f). **(g)** Intensity ratio plot of DnaJB1 alone and in the presence of $Hsp70^{\Delta EEVD}$. High intensity ratios indicate lack of interaction. **(h)** Intensity ratio plot of $Hsp70^{\Delta EEVD}$ bound over free $DnaJB1^{\Delta H5}$. Strong interaction is detected between the J-domain residues of $DnaJB1^{\Delta H5}$ and $Hsp70^{\Delta EEVD}$.

Figure 4: DnaJB1 JD-GF inhibition is essential for amyloid disaggregation

(a,b) Mechanistic model of Hsp70 interaction with- and activation by class A **(a)** and class B **(b)** JDPs. **(c)** Refolding of luciferase by Hsp70 and $Hsp70^{\Delta EEVD}$ measured in the absence (grey) and presence of DnaJA2 (blue), DnaJB1 (red), $DnaJB1^{E50A}$ (orange), $DnaJB1^{F102A}$ (yellow), or $DnaJB1^{\Delta H5}$ (purple). Hsp110 was included in all assays as a NEF. Reactivation after 120 min is shown as a percentage of native luciferase activity. Data are mean±s.e.m, (n=3). **(d)** Disaggregation of preformed α-synuclein fibers by Hsp70 and $Hsp70^{\Delta EEVD}$ measured in the absence (black) and presence of $DnaJB1^{WT}$ (red), $DnaJB1^{E50A}$ (orange), $DnaJB1^{F102A}$ (yellow), or $DnaJB1^{\Delta H5}$ (purple), with Hsp110 included in all reactions as a NEF. Decrease in ThT fluorescence reports on disaggregation of α-synuclein fibers. **(e)** Disaggregation of α-synuclein fibers by Hsp70 and $DnaJB1^{\Delta H5}$ with increasing concentrations of Hsp110 (200-1600 nM, light to dark purple). The fold excess of Hsp110 relative to 100nM is indicated. Disaggregation by $DnaJB1^{WT}$ with the lowest concentration of Hsp110 (100nM, red) and by DnaJA2 with the highest concentration of NEF (1600nM, blue) are also shown for comparison.

Methods

Labeling and purification of J-domain and JD-GF constructs of DnaJA1, DnaJA2, and DnaJB1

DnaJA1^{JD} (res 1-69), DnaJA1$^{JD\text{-}GF}$ (res 1-109), DnaJA2^{JD} (res 1-71), DnaJA2$^{JD\text{-}GF}$ (res 1-115), DnaJB1^{JD} (res 1-72), DnaJB1$^{JD\text{-}GF}$ (res 1-111), and DnaJB1$^{1\text{-}96}$ (res 1-96) wild type and mutant constructs were expressed in BL21(DE3) cells and grown in M9-minimal media supplemented with $^{15}NH_4Cl$ or $^{15}NH_4Cl/^{13}C$-glucose for ^{15}N or $^{15}N,^{13}C$ labeled sample, respectively. Cells were grown at 37 °C to an OD of 1.0 and induced overnight at 25 °C with 1mM IPTG.

All proteins were expressed with an N-terminal 6xHis-Smt3-tag purified on a HisTRAP column (GE Healthcare). The tag was subsequently cleaved using Ulp1 enzyme overnight at 4 °C, and the cleaved protein was further separated from the uncleaved protein and the enzyme using HisTRAP affinity column. The untagged protein was then concentrated and loaded onto a size exclusion Superdex 75 16/60 column (GE Healthcare) equilibrated with 50 mM Hepes, 100 mM KCl, pH 7.4, 2 mM DTT, and 0.03% NaN_3. Purity and composition of the proteins were confirmed by SDS-PAGE and ESI-MS.

Labeling and purification of full length Hsp70, DnaJA2, and DnaJB1 proteins

Hsp70 (HSPA8) or Hsp70 variants were expressed in *Escherichia coli* BL21CodonPlus (DE3)-RIPL cells transformed with pET-sumo plasmids. Full-length DnaJB1 variants were expressed in BL21 (DE3) cells. The cells were grown at 37 °C in M9 D_2O media, supplemented with $[^2H,^{12}C]$-glucose as the sole carbon source. Methyl labeling of the Ile-δ_1-$[^{13}CH_3]$, Val/Leu-$[^{13}CH_3, ^{12}CD_3]$, and Met-ε-$[^{13}CH_3]$ variety (referred to as ILVM) was achieved following the procedure of Tugarinov et al [7] and Gelis et al [33].

Stereospecific labeling of DnaJB1 Leu-δ_2-$[^{13}CH_3]$ and Val-γ_2-$[^{13}CH_3]$ was performed by addition of 240 mg/L of 2-$[^{13}C]$methyl-4-$[^2H_3]$-acetolactate [34] (NMRBio) at OD 0.9. After 45 minutes, isoleucine precursors and $^{13}CH_3$-labeled methionine were added, and 15 minutes afterwards protein production was induced by 1mM IPTG for 16 hours at 25 °C.

Unlabeled Hsp70, DnaJA2, DnaJB1 proteins or their variants were grown in Luria Bertani Broth (LB) medium to OD 0.8 and induced overnight with 1mM IPTG at 25 °C.

All constructs were expressed with an N-terminal 6xHis-Smt3-tag. Following expression, bacteria were harvested and lysed by French press, and the proteins were purified on a HisTRAP column (GE Healthcare), followed by cleavage of the purification tag using Ulp1 protease at 4 °C. The cleaved proteins were concentrated and loaded onto HiLoad 16/60 Superdex 200 pg gel filtration column (GE Healthcare) equilibrated with 25 mM Hepes pH 7.5, 150 mM KCl, and 0.03% NaN_3. Subsequently, proteins were concentrated, aliquoted, snap frozen in liquid nitrogen and stored at -80 °C. Purity of all proteins was confirmed by SDS-PAGE.

NMR spectroscopy

All NMR experiments were carried out at 25 °C on 14.1T (600 MHz), 18.8T (800 MHz), or 23.5T (1000 MHz) Bruker spectrometers equipped with triple resonance single (z) or triple (x,y,z) gradient cryoprobes. The experiments were processed by NMRPipe [35] or Bruker TopSpin, and analyzed via Sparky[36] or CCPNMR[37]. All NMR experiments involving Hsp70 protein, were carried out with the ATPase deficient T204A mutant of Hsp70 and in the presence of an ATP regenerating system[38,39].

Assignments of J-domain and DnaJB1$^{JD\text{-}GF}$ constructs

Backbone ^{1}H, ^{15}N and ^{13}C resonance assignments were carried out on a sample of DnaJB1^{JD}, DnaJB1$^{JD\text{-}GF}$, or DnaJA2^{JD} in 50mM Hepes pH 7.5, 50 mM KCl, 0.03% NaN_3 and 10% D_2O buffer. DnaJB1^{JD} and DnaJB1$^{JD\text{-}GF}$ were assigned using a set of 3D HNCACB, CBCA(CO)NH and HN(CA)CO experiments [40,41] recorded on a 600 MHz magnet, resulting in the unambiguous assignment of 68 out of 68 non-proline residues for DnaJB1^{JD} and 94 out of 104 for DnaJB1$^{JD\text{-}GF}$. DnaJA2^{JD} assignments were obtained using 3D HNCACB, CBCA(CO)NH, HN(CA)CO and HNCO experiments acquired at 800 MHz, resulting in the assignment of 71 out of the 74 non-proline residues. The assignments of DnaJA1^{JD} were available through the BMRB (ID 19163).

Side-chain chemical shift assignments for DnaJB1$^{JD\text{-}GF}$ were obtained using (H)C(CO)NH-TOCSY, H(CCO)NH-TOCSY[42,43], HCCH-TOCSY, $(H_\beta)C_\beta(C_\gamma C_\delta)H_\delta$[44], $(H_\beta)C_\beta(C_\gamma C_\delta C_\varepsilon)H_\varepsilon$[44], ^{13}C-NOESY-HSQC, and ^{15}N-NOESY-HSQC experiments on

^{15}N,^{13}C- DnaJB1JD-GF sample. Overall 72% of ^{1}H, 85% of ^{13}C, and 69% of ^{15}N resonances were assigned.

Chemical shift assignments for DnaJB1 methyl groups

Methyl-TROSY spectra[6] were recorded on per-deuterated protein samples dissolved in 100% D_2O, 25 mM Hepes, pH 7.5, 50 mM KCl, and 0.03% NaN_3.

The assignment of DnaJB1^{JD-GF} methyl residues were obtained via (H)C(CO)NH-TOCSY, H(CCO)NH-TOCSY [42,43], and methyl–methyl NOE experiments[45].

In order to assign the methyl residues of DnaJB1 CTDs (res 154-340) fifteen Ile to Leu or Leu/Val to Ile point mutations were made (I175L, I197L, I203L, V236I, L262I, L276I, V283I, V288I, V297I, L302I, L304I, I316L). A combined analysis of methyl-TROSY spectra of mutant and wild-type (wt) proteins and a 3D methyl-methyl NOESY data set (mixing time of 200 ms; correlations of the form ($^{13}C_j$-NOE-$^{13}C_k$-$^{1}H_k$) were recorded[46]). The observed pattern of intra- and intermolecular NOEs was carefully compared with the network of short-range methyl–methyl distances in the crystal structure (3AGY [47]). Stereospecific assignment of Val and Leu methyl groups was achieved by labelling only the δ_2-Leu and γ_2-Val moieties (proS labeling; NMRBio)[34]. DnaJB1$^{1-325}$ construct lacking the dimerization domain was used to distinguish between inter- and intra-dimer NOEs, as well as to validate the assignments of the dimerization domain methyl groups. These combined approaches allowed unambiguous assignment of 95 out of 99 methyl peaks (64 methyl residues).

Backbone dynamics

Measurements of backbone ^{15}N R_1 and R_2 relaxation rates and steady-state heteronuclear ^{1}H-^{15}N NOEs (hNOEs) were carried out on a 3 mM uniformly ^{15}N-enriched DnaJB1^{GF} sample at 25°C, pH 7.4, 18.8 T using heat-compensated ^{1}H-^{15}N HSQC based pulse schemes [48]. The ^{15}N R_1 data were acquired using relaxation delays ranging from 2-1500 ms while ^{15}N $R_{1\rho}$ rates were quantified using relaxation delays from 2-100 ms. R_2 values were calculated from R_1 and $R_{1\rho}$ rates according to the equation $R_{1\rho} = R_1\cos^2\theta + R_2\sin^2\theta$, where $\theta = \arctan(\omega_{SL}/\Delta\omega)$, $\Delta\omega$ is the resonance offset from the spin-lock carrier and ω_{SL} is the

spin-lock field strength (1.0 kHz). Values of relaxation rates were obtained by non-linear least-squares fitting of the experimental data to a mono-exponential decay function, Aexp(-R_iT), R_i={R_1,$R_{1\rho}$}. ^{1}H-^{15}N NOE values were calculated by comparing the peak intensities with and without ^{1}H saturation of 6 s.

Values of R_1, R_2 and NOE were fitted using the model-free approach with ModelFree4 software[49] assuming isotropic overall motion, to extract a single correlation time (τ_C) of 9.5 nsec and residue specific values of order parameters (S^2).

Paramagnetic relaxation enhancement (PRE) measurements

Labeling of DnaJB1$^{JD\text{-}GF}$ with spin-label was achieved by introducing a single cysteine mutation at the desired position (G40, S56, or G108). Purified mutants, stored in 5mM DTT, were buffer-exchanged into 1 mL of degassed buffer (25 mM Hepes, pH 7.5, 50 mM KCl, 1 mM EDTA, 0.03% NaN_3), prior to incubation overnight at 4°C with 3-fold molar excess of MTSL spin label (Toronto Research Chemicals *S*-(2,2,5,5-tetramethyl-2,5-dihydro-1H-pyrrol-3-yl)methyl methanesulfonothioate). The labeling reaction was terminated by exchanging the sample into the NMR buffer. All samples were submitted for mass confirmation (ESI-MS) to ensure proper labeling and complete labeling was achieved for all constructs.

The reduced samples were generated through the addition of 100 mM ascorbic acid, pH 7.4 at 4 °C overnight, followed by buffer exchange to the NMR buffer.

Amide ^1H_N relaxation rates were recorded in the oxidized (R_2^{ox}) and reduced (R_2^{red}) states to obtain the PRE rate, $\Gamma_2 = R_2^{ox} - R_2^{red}$. Relaxation rates were measured using a ^{1}H-^{15}N HSQC pulse sequence at 800 MHz using a ten-point measurement, ranging from 0 to 40 ms [28]. Measured peak intensities in two-dimensional correlation maps were fitted to extract R_2, with errors estimated from the covariance matrix method [50].

Correlations disappeared for some residues in the oxidized state; in these cases a lower bound for R_2^{ox} was estimated from the relation

$$\frac{I_{ox}}{I_{red}} = \frac{\exp(-2R_2^{ox}\tau)}{\exp(-2R_2^{red}\tau)} \cdot \left(\frac{R_2^{red}}{R_2^{ox}}\right)^2 \qquad [1]$$

where I_{red} is the intensity of the correlation in the ^{15}N-^{1}H spectrum recorded of the protein

with the spin label in the reduced state while I_{ox} is set to 3 times the noise floor. The value τ is the time for transfer of magnetization between ^{1}H and ^{15}N spins and is set to 5.3 ms. No significant changes in R_2 rates were obtained from back-to-back measurements (differences were within experimental errors) and mass-spectrometric analysis showed that samples with the MTSL spin-label remained attached to the protein after each experiment. Site-specific methyl ^{1}H Γ_2 rates were converted to distances from the proton in question to the paramagnetic centre using the formula [27]:

$$r = \left[\frac{\beta}{\Gamma_2} \left(4\tau_c + \frac{3\tau_c}{1+\omega_H^2 \tau_c^2} \right) \right]^{1/6} \qquad [2]$$

where $\beta = 1.23 \cdot 10^{-44}$ m^6 s^{-2}, $\omega_H = 2\pi 800 \cdot 10^6$ rad s^{-1} and τ_c is set to 9.5 ns (calculated through backbone relaxation data) .

Distance constraints were calculated for each construct, resulted in 88 constraints in total.

Residual dipolar coupling (RDC) measurements

Backbone amide $^{1}D_{NH}$ RDCs were measured using a 300 μM sample of DnaJB1 JD-FG aligned in 4.2% v/v $C_{12}E_6$ PEG/*n*-hexanol (Sigma) or 16 mg/mL bacteriophage pf1 (Asla Scientific). The sample was diluted in 50 mM Hepes pH 7.4, 150 mM NaCl buffer as a higher salt concentration was necessary to reduce the strength of electrostatic interactions between the alignment medium and the protein. $^{1}D_{NH}$ RDCs were measured using IPAP (in-phase anti-phase) HSQC experiments[51] on a 1000 MHz Bruker spectrometer and ranged from +30 to -18 Hz.

CS-Rosetta calculations

Structure of the DnaJB1$^{JD\text{-}GF}$ was generated using CS-Rosetta[52-54].

As a first step, the pick-fragments application from the CS-Rosetta toolbox 3.0 was used for fragment selection, based on the backbone chemical shift data[55]. Overall, 546 chemical shifts were used as input (95 $^{13}C_\alpha$ shifts, 84 $^{13}C_\beta$ shifts, 95 $^{13}C'$ shifts, 94 ^{15}N shifts, 94 $^{1}H_N$ shifts, and 84 $^{1}H\alpha$ shifts). The fragment library containing 3- and 9-residue fragments was assembled by scoring both against a library of fragments with chemical shifts predicted from SPARTA+ [56], and against chemical shifts predicted from secondary structure elements.

We then used Rosetta's Ab initio Relax protocol with the chemical shifts, 1271 NOEs and 88 distance restraints derived from $^{1}H_{N}$ PRE measurements as inputs, to generate 250,000 starting models. Only PRE constraints were included in the preliminary centroid mode step.

The resulting lowest energy 500 models (by total score) were then subjected to local simultaneous refinement of backbone and side chain conformations (Rosetta-relax), incorporating 95 residual dipolar coupling meassurements (RDC). Each such run generated 500 models, with the same constraints as the original ab initio modeling. The top 10 models of the resulting ~250,000 models (by total score) are shown in Fig 1e of the main text and submitted to the PDB (accession number 6Z5N). Quality analysis of the structures was performed using PSVS 1.5 validation software suite[57] and PROCHECK-NMR [58].

NMR chemical shift perturbations

The interaction of DnaJB1 with Hsp70 or Hsp70 C-terminal peptide (the last 20 amino acid of the Hsp70; GGGAPPSGGASSGPTIEEVD) was monitored by 2D ^{1}H–^{13}C HMQC methyl-TROSY experiments[6]. Deuterated Hsp70 protein (400 μM) or unlabeled Hsp70 peptide (800 μM) was added to methyl labeled DnaJB1 samples (200 μM monomer concentration).

CSPs were calculated from the relation

$$\Delta\delta = \sqrt{\left(\frac{\Delta\delta_H}{\alpha}\right)^2 + \left(\frac{\Delta\delta_C}{\beta}\right)^2} \quad [3]$$

where $\Delta\delta_{H(C)}$ is the shift change between methyl group ^{1}H (^{13}C) nuclei in apo and fully saturated forms of the protein, α (β) is one standard deviation of the methyl ^{1}H (^{13}C) chemical shifts (separate values of α (β) are used for different methyl groups), as tabulated in the Biological Magnetic Resonance Data Bank (www.bmrb.wisc.edu). CSPs greater than one standard deviation from the mean were considered significant.

NMR titrations

To estimate dissociation constants for the interaction of the DnaJB1 with Hsp70 or Hsp70 C-terminal peptide (GGGAPPSGGASSGPTIEEVD), U-[^{2}H,$^{13}CH_3$]-DnaJB1 samples (200 μM) were titrated with increasing amounts of deuterated Hsp70 (50, 100, 150, 200, 300, 500, and 800 μM) or unlabeled C-terminal peptide (20, 40, 80, 120, 160, 200, 240, 280,

320, 360, 400, 480, 600, 1000, and 1650 μM), and the positions of cross-peaks monitored by recording 2D ^{1}H-^{13}C HMQC spectra.

The K_d values for these titrations were calculated by a nonlinear least-squares analysis using the equation

$$\Delta\delta' = \Delta\delta'_{MAX}\frac{[L]_T + [P]_T + K_D - \sqrt{([L]_T + [P]_T + K_D)^2 - 4[P]_T[L]_T}}{2[P]_T} \quad [4]$$

where $[P]_T$ and $[L]_T$ are the total protein (NMR labeled) and ligand (unlabeled) concentrations at each aliquot, Δδ' is the change in peak position after each aliquot and $\Delta\delta'_{MAX}$ is the change in shifts between apo and fully bound states of the protein. Binding isotherms were quantified separately for ^{1}H and ^{13}C chemical shifts.

Hsp70 ATPase activity determination

Hsp70 phosphate release rates following ATP hydrolysis were measured under steady state conditions by monitoring the change in fluorescence of the phosphate binding protein (PBP) A197C mutant, which was labelled at Cys197 using 7-Diethylamino-3-[N-(4-maleimidoethyl)carbamoyl]coumarin (MDCC, CDX-D0198 from Adipogen). Fluorescence was measured in a Synergy H1 plate reader by exciting at 430nm and measuring at 465nm.

All reactions contained PBP, 0.25μM Hsp70 in 50mM HEPES pH 7.5, 25mM KCl, 10mM $MgCl_2$, and 2 mM DTT, and varying concentrations (2.5, 10, 50, 100, 125, 250, and 500 nM) of the JDPs. After the plate was incubated at 37 °C for 10 minutes, the reactions were started by injection of 100 μM ATP to each well. Wells were then read every 40 s for the first 20 min, and every 2 min for the following 40 min. For each plate, a series of five phosphate concentrations with PBP alone was measured to generate a calibration curve, which was used to correlate fluorescence to concentration of the released phosphate. All ATPase assays were performed in triplicate.

Protein refolding

Recombinant firefly luciferase (0.2 μM) was incubated for 40 min at 30 °C in denaturation buffer (25 mM HEPES-KOH, pH 7.5, 50 mM KCl, 10 mM $MgCl_2$, 2 mM DTT, 6 M Guanidinium chloride). To start the refolding reaction the denatured luciferase was diluted

150 fold into refolding buffer (25 mM Hepes, pH 7.5, 50 mM KCl, 10 mM $MgCl_2$, 1 mM DTT, 0.1 mg/ml BSA, 1mM ATP, 20 mM creatine phosphate, 6 µg creatine kinase) supplemented with the indicated chaperones and incubated at 30°C. Luminescence was measured after 0, 10, 20, 40, 80 and 120 minutes by addition of 50 µM of luciferase reagent (Promega) to 9 µl of the refolding reaction on a Synergy H1 plate reader. The concentration of Hsc70 and Hsp110 was kept constant at 2 and 0.1µM, respectively. The JDP concentration used in each condition is indicated below:

DnaJB1:Hsp70 (0.5:1), DnaJB1$^{\Delta H5}$:Hsp70 (0.2:1), DnaJB1^{E50A}:Hsp70 (0.5:1), DnaJB1^{F102A}:Hsp70 (0.5:1), DnaJB1:Hsp70$^{\Delta EEVD}$ (2:1), DnaJB1$^{\Delta H5}$:Hsp70$^{\Delta EEVD}$ (2:1), DnaJB1^{E50A}:Hsp70$^{\Delta EEVD}$ (2:1), DnaJB1^{F102A}:Hsp70$^{\Delta EEVD}$ (2:1), DnaJA2:Hsp70 (0.5:1), DnaJA2:Hsp70$^{\Delta EEVD}$ (0.5:1)

Fluorescence resonance energy transfer (FRET) experiments

Fluorescent labeling of Hsp70 S494C and Hsp70ΔEEVD S494C was performed at position 494 (S494C) in an otherwise cysteine-free background (C267A, C574A, C603A) and purified as described. Prior to labeling, chaperones were incubated with 10 mM DTT for 30 min, followed by exchange into a reducing agent free buffer by passing the protein through a desalting column (PD MiniTrap™ G-25, GE Healthcare). Labeling was achieved by incubating the proteins with 10-fold molar excess of Alexa Fluor™ 488 C5-maleimide (Invitrogen) or Alexa Fluor™ 594 C5-maleimide (Invitrogen) fluorescent dye for 2 hours at 25 ºC and in the presence of 0.5 mM TCEP. Excess label was removed by a desalting column (PD MiniTrap™ G-25, GE Healthcare). Labelling efficiencies were determined by absorbance and exceeded 90%.

FRET experiments were performed with 200 nM of mixed donor (AF488) and acceptor (AF594) and incubated with 20 µM α-synuclein fibrils and indicated J-domain proteins in 50mM Hepes-KOH pH 7.5, 50 mM KCl, 5 mM MgCl2, 2 mM DTT and 2 mM ATP. Samples were allowed to equilibrate for 1 hour at 25 ºC. Emission spectra between 500 and 700 nm were recorded using a CLARIOstar plate reader (BMG LABTECH) at an excitation centered at 480 nm with a bandwidth of 10nm and emission bandwidth of 10nm. FRET efficiencies were determined from the ratios between donor and acceptor fluorescence I(618nm)/I(518nm).

To quantify the effect of the different J-domain proteins on Hsp70 clustering, FRET efficiencies were measured in the presence of an excess of the indicated JDP (5 μM) and expressed as a fraction of the FRET efficiency measured with a sub-stoichiometric concentration of the same JDPs (200 nM).

Fluorescence anisotropy measurements

Steady-state equilibrium binding of DnaJA2, DnaJB1, and DnaJB1$^{\Delta H5}$ chaperones to preformed α-synuclein fibers was measured by fluorescence anisotropy using 200 nM of fluorescently tagged chaperones (DnaJB1 G194C-AF594, DnaJB1$^{\Delta H5}$ G194C-AF594, or CCGPCC-DnaJA2-FLASH [59]). Samples were allowed to equilibrate for 1 hour at 22 ºC and data was acquired by a CLARIOstar plate reader (BMG LABTECH) with excitation at 590nm with a bandwidth of 50nm, emission at 675 with a bandwidth of 50nm and dichroic filter of 639nm for AF594 detection and excitation at 482 with a bandwidth of 16 nm, emission at 530 with a bandwidth of 40 nm and a dichroic filter at 504nm for FLASH detection. Data were fit to a one-site binding model using Graphpad prism 6.

Steady-state equilibrium binding of DnaJB1 and DnaJB1$^{\Delta H5}$ to Hsp70 T204A was measured by fluorescence anisotropy using 25 nM of fluorescently tagged chaperones (DnaJB1 G194C-AF488, DnaJB1$^{\Delta H5}$ G194C-AF488). Samples were allowed to equilibrate for 30 minutes at 37 ºC and measurements were performed on a Tecan SPARK 10M plate reader in black, flat-bottomed 384 square well plates. Excitation filter was centered on 485 nm with a bandwidth of 20 nm, and emission filter was centered on 535 nm with a bandwidth of 25 nm. Data were fit to a one-site binding model using OriginPro version 2018.

Steady-state equilibrium binding of Hsp70 to α-synuclein fibrils as a function of JDP concentration was measured by fluorescence anisotropy using 200nM of fluorescently tagged Hsp70 S494C-AF488 (C267A, C574A, C603A) preincubated for 1 hour at 22 ºC with 2 uM preformed asyn fibrils and the indicated concentrations of DnaJB1, DnaJB1$^{\Delta H5}$ or DnaJA2. Anisotropy measurements were performed in a CLARIOstar plate reader

(BMG LABTECH) with excitation at 482 with a bandwidth of 16 nm, emission at 530 with a bandwidth of 40 nm and a dichroic filter at 504nm.

Co-sedimentation assay

10uM Hsp70 and 10uM preformed α-synuclein fibrils were incubated with the indicated concentration of DNAJB1, DnaJB1$^{\Delta H5}$ or DnaJA2 and 2mM ATP for 1 hour at 22 ºC. Samples were centrifuged at 10,000g for 10min, supernatant removed and pellets gently washed with buffer (50 mM Hepes-KOH (pH 7,5), 50 mM KCl, 5 mM $MgCl_2$ and 2 mM DTT). The content of the pellet fractions was analysed by SDS-PAGE.

Disaggregation assay

Disaggregation of amyloid fibrils by chaperones was monitored by changes in Thioflavin T (ThT) fluorescence over a 12-16 hours period using a FLUOstar Omega plate-reader (BMG LABTECH), excitation at 440nm, emission at 480 nm. 1 µM preformed α-synuclein fibrils[12] were incubated with 2 µM Hsp70, 1 µM DnaJB1, 0.1 µM Hsp110 (unless indicated otherwise), 2 mM ATP, an ATP regeneration system (8 mM PEP and 20 ng/µL pyruvate kinase), and 30 µM ThT at 30 ºC in 50 mM Hepes-KOH (pH 7,5), 50 mM KCl, 5 mM $MgCl_2$ and 2 mM DTT. Background ThT fluorescence of buffer and chaperones was subtracted, and all intensities were normalized to the fluorescence intensity at t=0 min. Data shown are representative traces of 3 independent experiments.

Reporting summary

Further information on research design is available in the Nature Research Reporting Summary linked to this paper.

Acknowledgements

The authors would like to thank T. Scherf for NMR support and the Clore Institute for High-Field Magnetic Resonance Imaging and Spectroscopy. We also thank D. Fass for helpful discussions and advice.

R.R. is supported by the European Research Council starting grant (ERC-2018-STG 802001), the Minerva Foundation, and a research grant from the Blythe Brenden-Mann New Scientist Fund. BB is supported by the Deutsche Forschungsgemeinschaft grant (SFB 1036, BU617/19-1) and the Helmholtz-Gemeinschaft (German-Israeli Helmholtz Research School in Cancer; AmPro) to BB and RR. M.M acknowledges the support of the Helmholtz International Graduate School for Cancer Research at the DKFZ. N.L. is the incumbent of the Alan and Laraine Fischer Career Development Chair, and is supported by the Israel Science Foundation (grant No. 2462/19)

Contributions

O.F., M.A-A., A.W., N.N., and R.R. designed the research; O.F., M.A-A. and M.M. performed the NMR spectroscopy measurements, processed and analyzed the data. M.A-A. determined NMR structure of DnaJB1-JD-GF together with N.L., and R.R.; O.F., A.W., N.N., and M.M. performed the biochemical and functional assays; O.F., M.A-A., A.W., M.M., N.N., B.B. and R.R. analyzed data; and O.F., M.A-A., M.M., A.W., N.N., B.B., and R.R. wrote the paper.

Corresponding authors

Correspondence and requests for materials should be addressed to Rina Rosenzweig or Bernd Bukau.

Competing interests

The authors declare no competing interests.

Additional Information

Supplementary information containing Supplementary Table 1 and Supplementary Fig. 1 is available for this paper.

Correspondence and requests for materials should be addressed to R.R or B.B.

Data availability

The data that supports the findings of this study are available from the corresponding authors upon request. NMR chemical shifts have been deposited in the Biological Magnetic Resonance Data Bank (BMRB) under the following accession codes: 50169 for DnaJB1^{JD}, 50168 for DnaJA2^{JD}, and 50167 for DnaJB1$^{JD\text{-}GF}$. The structure of DnaJB1$^{JD\text{-}GF}$ has been deposited to the Protein Data Bank (PDB), accession code: 6Z5N.

Supplementary Information

This file contains Supplementary Table 1 (NMR and refinement statistics for DnaJB1$^{JD\text{-}GF}$ structure) and Supplementary Fig. 1 (Image of an uncropped gel used in Extended Data Fig. 10g).

Extended Data Figure Legends

Extended Data Figure 1: Interaction of JDP J-domains with Hsp70 chaperone.

(a-c) Residue-resolved NMR signal intensity ratios I/I_0, where I and I_0 are signal intensities for Hsp70-bound and free, $DnaJA2^{JD}$ **(a)**, $DnaJB1^{JD}$ **(b)**, and $DnaJA1^{JD}$ **(c),** respectively. The positions of the four helices in each J-domain are indicated at the bottom of the plot. Large changes in intensity are detected at the end of helix II, the flexible loop containing the conserved HPD motif, and at helix III, corresponding to Hsp70-binding sites. In all three J-domains, similar residues are involved in binding, pointing to high conservation of JD-Hsp70 interaction. **(d)** Overlay of $^{1}H–^{15}N$ HSQC spectra of 0.2mM $DnaJA1^{JD\text{-}GF}$ alone (in black), and in the presence of two-fold excess of protonated (^{1}H) Hsp70 (green). Upon complex formation with Hsp70, the majority of the J-domain peaks were broadened out beyond detection, while the GF residues that are part of a flexible disordered linker were not affected, indicating that only the J-domain, and not the GF rich region, interacts with the Hsp70 chaperone. Assignments of J-domain residues are indicated on the spectrum. **(e)** $^{1}H–^{15}N$ HSQC spectra of 0.2mM $DnaJB1^{JD}$ alone (in black), and in the presence of two-fold excess protonated (^{1}H) Hsp70 (red). Here too, addition of protonated Hsp70 causes severe peak broadening in the majority of the J-domain residues, with the exception of the flexible terminal residues and side chains. This, however, is in striking contrast to the spectrum of $DnaJB1^{JD\text{-}GF}$ under the same conditions (Fig. 1f of the main text), which showed no peak broadening, indicating lack of interaction with Hsp70. **(f)** Comparison of chemical shifts of residues 1-71 in the $DnaJB1^{JD}$ and the same residues in the $DnaJB1^{JD\text{-}GF}$ construct. The differences in the chemical shift positions ($\Delta\delta$) are defined by the relation

$\Delta\delta = \sqrt{(\Delta\delta_H)^2 + \left(\frac{\Delta\delta_N}{5}\right)^2}$, where, where $\Delta\delta_H$ and $\Delta\delta_N$ are ^{1}H proton and ^{15}N nitrogen shift changes between the chemical shifts of $DnaJB1^{JD}$ and $DnaJB1^{JD\text{-}GF}$ residues (1-71). Large chemical shift changes are seen in residues of helix II and III, which are colored red on the structure of DnaJB1 J-domain. Residues displaying large differences between $DnaJB1^{JD}$ and $DnaJB1^{JD\text{-}GF}$ are the same ones that show changes upon Hsp70 binding (helix II and III), and those in helix IV.

Extended Data Figure 2: Structural characterization of $DnaJB1^{JD\text{-}GF}$

(a) $TALOS^{+}$ secondary structure probabilities[20] of $DnaJB1^{JD\text{-}GF}$ derived from backbone $^{13}C_\alpha$, $^{13}C_\beta$, $^{13}C'$, ^{15}N, and $^{1}H_N$ chemical shifts. Predicted α-helices are shown in red and β-sheets in blue. **(b)** Backbone order parameters (S^2) calculated using ModelFree[49] from ^{15}N relaxation data (see methods). The location of the five helices in $DnaJB1^{JD\text{-}GF}$ and their boundaries is indicated above the plot. **(c)** Backbone amide RDCs ($^{1}D_{NH}$) collected in 16 mg/mL phage pf1 alignment media. **(d-f)** $^{1}H_N$ PRE (R_2^{ox}-R_2^{red}) profiles recorded for

nitroxide spin-labeled DnaJB1$^{JD\text{-}GF}$ with the MTSL spin-label located at residues 108 **(d)**, 56 **(e)**, and 40 **(f)**. ^{1}H-^{15}N cross-peaks that are broadened beyond detection in the oxidized state and were calculated to have a PRE ≥ 200 (see methods) are shown as grey bars. **(g)** Correlation between observed RDCs in pf1 alignment media and those calculated for the 10 lowest energy CS-ROSETTA[52-54] structures. The RDC R-factor, Rdip, is given by

$R_{dip} = \{\langle (D_{obs} - D_{cal})^2 \rangle / (2\langle {D_{obs}}^2 \rangle)\}^{1/2}$, where D_{obs} and D_{cal} are the observed and calculated RDC values, respectively. Da and η are the magnitude (normalized to the N-H RDCs) and rhombicity, respectively, of the alignment tensor. **(h)** Select strips from a 3D NOESY-HSQC experiment depicting long range methyl-NH NOEs for residues 28-102 (left), 29-106 (middle), and 101-56 (right), and indicating long range interactions between helix V and helices II and III.

Extended Data Figure 3: Deletion of helix V removes the GF inhibition of the J-domain and restores Hsp70 binding

(a) Overlay of ^{1}H-^{15}N HSQC correlation maps of 0.2mM DnaJB1$^{1\text{-}96}$ alone (black), and in complex with 0.2mM Hsp70 (red). Deletion of helix V residues restores the ability of DnaJB1 J-domain to interact with Hsp70, even in the presence of the GF region. **(b)** Differences in chemical shifts between DnaJB1^{JD} (res 1-71) and DnaJB1$^{1\text{-}96}$ construct lacking helix V. No significant changes in the spectra were observed between the two constructs, with the exception of residues located in helix IV (colored red on the structure of DnaJB1 J-domain), which connects the JD and GF. **(c)** ^{1}H–^{13}C HMQC spectra showing the leucine\valine (left) and isoleucine (right) regions of 0.2mM $^{13}CH_3$-ILVM labeled full-length DnaJB1 (grey), DnaJB1^{JD} (red), and DnaJB1$^{JD\text{-}GF}$ (orange). The DnaJB1$^{JD\text{-}GF}$ peaks overlap with those of full length DnaJB1 (with the exception of small CSPs observed for residues 29 and 48), while those of free JD do not, indicating that in the full length protein the J-domain is in the while those of free JD do not, indicating that in the full length protein the J-domain is in the GF-inhibited conformation.

Extended Data Figure 4: Interaction of DnaJB1 with Hsp70

(a) Chemical shift perturbations induced by Hsp70 binding to [^{2}H, $^{13}CH_3$-ILVM]-labelled DnaJB1. CSPs are defined by the relation $\Delta\delta = \sqrt{\left(\frac{\Delta\delta_H}{\alpha}\right)^2 + \left(\frac{\Delta\delta_C}{\beta}\right)^2}$, where $\Delta\delta_H$ and $\Delta\delta_C$ are methyl ^{1}H and ^{13}C chemical shift changes between apo and bound forms of the protein, and α (β) is one standard deviation from the methyl ^{1}H (^{13}C) chemical shifts deposited in the Biological Magnetic Resonance Data Bank (α is 0.29 (I), 0.28 (L), 0.27 (V) and 0.41 (M), whereas β is 1.65 (I), 1.6 (L), 1.4 (V), and 1.54 (M)). While Hsp70 binds to two sites in DnaJB1 (J-domain and CTDI), large chemical shifts changes are observed only in CTDI, indicating that this domain binds to Hsp70 in a transient manner (on a fast NMR time

scale). **(b)** Per-residue peak intensity ratios of DnaJB1^{32QPN34}, in the absence, and presence of Hsp70 chaperone. In this variant, conserved residues (32-34) in the J-domain HPD motif, which is essential for Hsp70 activation, were mutated to QPN. Upon addition of Hsp70, no changes in intensities were detected for the J-domain residues, indicating that, as expected, mutations to the HPD motif abolish the J-domain-Hsp70 interaction[60,61]. The DnaJB1 CTDI interaction with Hsp70, however, remained strong and was unaffected by the mutation. **(c)** Peak intensity ratios of DnaJB1 CTDs (res 154-340) alone, and in complex with Hsp70 chaperone. The interaction of Hsp70 with the CTDI of DnaJB1 occurs independently of the JD. **(d)** Differences in chemical shifts between free DnaJB1 and DnaJB1 in complex with a synthetic peptide corresponding to the last 20 amino acids of the Hsp70 C-terminal tail. Large chemical shift perturbations are detected in the CTDI region of DnaJB1, similar to those observed upon DnaJB1 binding to full length Hsp70 (see panel a).

Extended Data Figure 5: Hsp70 binds to the CTDI of DnaJB1 but not of DnaJA2

(a-f) Overlay of ^{1}H-^{13}C HMQC correlation maps of ILVM-labeled Hsp70 (black) and Hsp70 in complex with DnaJB1 **(a,** light red**)**, DnaJB1 J-domain **(b,** dark red**),** and DnaJB1 CTDs **(c,** cyan**)**. DnaJB1 J-domain interacts with residues in Hsp70 NBD and SBD, similarly to the interaction observed between *E.coli* DnaK and DnaJ J-domain. DnaJB1 CTDs, however, interact with a different region of Hsp70, corresponding to the disordered C-terminal tail of Hsp70. Interaction of ILVM-labeled Hsp70 with DnaJA2 **(d,** light blue**)**, DnaJA2 J-domain **(e,** dark blue**)**, and DnaJA2 CTDs **(f,** green**)**. The residues of DnaJA2 J-domain interact with similar Hsp70 residues as DnaJB1 J-domain, in both cases located at the interface between NBD and SBD. Unlike DnaJB1, however, no interaction was observed between DnaJA2 CTDs and Hsp70.

Extended Data Figure 6: Client proteins and the Hsp70 C-terminal EEVD tail bind simultaneously to DnaJB1

(a) Per-residue peak intensity ratios of DnaJB1 in complex with excess of α-synuclein over DnaJB1 alone. Lower ratios indicate greater changes between bound and free states. **(b)** Residues displaying significant changes in intensities (2 standard deviations below mean) are shown as yellow spheres on the structure of DnaJB1 CTDs (PDB ID 3AGX[29]). α-synuclein interacts predominantly with CTDII domain of the chaperone, with only minor changes being observed in CTDI residues. **(c-d)** Competition experiments between α-synuclein and a synthetic peptide corresponding to the last 20 aa in the Hsp70 C-terminal tail (EEVD peptide). DnaJB1 residues showing broadening upon interaction with α-synuclein are unaffected by addition of EEVD peptide **(c)**. Likewise, the behavior of DnaJB1 residues displaying shifts upon EEVD peptide binding was unchanged in the presence of α-synuclein **(d)**, indicating that DnaJB1 can interact simultaneously with both.

Extended Data Figure 7: Removal of the Hsp70 EEVD tail abolishes binding to class B JDPs

(a) ^{1}H-^{13}C HMQC spectra of Hsp70 (pink) and Hsp70$^{\Delta EEVD}$ (black) showing the isoleucine **(a)** and valine **(b)** spectral regions. No conformational changes were detected in the Hsp70 chaperone upon deletion of the four C-terminal residues (EEVD). The only visible difference between the two spectra is the lack of the V645 peak in **(b)**, as this residue is part of the C-terminal tail that was deleted in Hsp70$^{\Delta EEVD}$. **(c,d)** Interaction of Hsp70$^{\Delta EEVD}$ with DnaJA2 **(c)** and DnaJB1 **(d)**. The interaction between DnaJA2 and Hsp70$^{\Delta EEVD}$ occurs via the same residues as between DnaJA2 and wt Hsp70 (**c**, blue; compare to Extended Data Figure 5c), while no interaction was detected between Hsp70$^{\Delta EEVD}$ and DnaJB1 (**d**, red)

Extended Data Figure 8: DnaJB1 mutants with released GF inhibition of the JD

(a-b) Cartoon representation of DnaJB1$^{JD\text{-}GF}$, highlighting the position of residues E50 **(a)** and F102 **(b)** that were mutated to alanines. F102A mutation was designed based on our DnaJB1$^{JD\text{-}GF}$ structure to disrupt the hydrophobic contacts between J-domain residues A28, L29, F45 and helix V. E50A mutation was previously reported (in Sis1) to rescue the defects in protein refolding activity of Hsp70$^{\Delta EEVD}$ [23,26] and we therefore suspected it also released the J-domain. **(c-d)** ^{1}H-^{15}N HSQC spectra of DnaJB1$^{JD\text{-}GF}$ E50A **(c)** and DnaJB1$^{JD\text{-}GF}$ F102A **(d)** alone, and in complex with Hsp70 (teal). While wt DnaJB1$^{JD\text{-}GF}$ was unable to bind Hsp70, partial release of the J-domain by targeted mutation in either the J-domain or GF region generates DnaJB1$^{JD\text{-}GF}$ constructs that bind Hsp70 with high affinity - as indicated by the severe broadening of the peaks in the bound spectrum. **(e-f)** Selected regions of the HSQC spectra showing residues D57 and D65 of DnaJB1$^{JD\text{-}GF}$ E50A **(e)** and F102A **(f)** in slow exchange between the GF-inhibited and released J-domain conformations. The population of each conformation was calculated by integrating the peak volumes, and is indicated for each residue. Overall, E50A mutation to the J-domain releases 64% while F102A mutation to the GF helix V releases 36%.

Extended Data Figure 9: DnaJB1 mutants with partially released JD can interact with Hsp70 lacking the C-terminal tail.

(a-c) Peak intensity ratios of DnaJB1 WT **(a)**, DnaJB1 F102A **(b)**, and DnaJB1 E50A **(c)** in the presence of 2-fold molar excess of Hsp70$^{\Delta EEVD}$ chaperone lacking the four last residues (EEVD) of the C-terminal tail. All plots are normalized, per residue, by the peak intensities of each of the DnaJB1 variants alone. WT DnaJB1 protein is unable to bind to

Hsp70$^{\Delta EEVD}$, as Hsp70 C-terminal is required for the release of its J-domain. However, both DnaJB1 mutants with partially released JDs bound to Hsp70, though the interaction was only through their J-domain, as the presence of Hsp70 C-terminal tail is required for binding of DnaJB1 CTDI **(d-e)**.

Extended Data Figure 10: Characterization of Hsp70 activity with constitutively JD-released (DnaJB1$^{\Delta H5}$) mutant

(a) Spectrum of DnaJB1$^{\Delta H5}$ mutant (purple), containing a released J-domain, overlayed onto the spectrum of WT DnaJB1(blue). Outside of the J-domain residues, no changes were observed to the overall conformation of the chaperone. **(b)** DnaJB1 J-domain residues L55 and V54 display different chemical shifts in the GF-inhibited (gray), and free J-domain (black) conformations. J-domain of DnaJB1$^{\Delta H5}$ mutant is shown to be fully released. **(c-d)** Steady-state ATPase activity of 250 nM Hsp70 **(c)** or Hsp70$^{\Delta EEVD}$ **(d)** chaperone measured in the presence of increasing concentrations of DnaJA2 (blue), DnaJB1 WT (red), DnaJB1^{E50A} (orange), DaJB1^{F102A} (yellow), or DnaJB1$^{\Delta H5}$ (purple) variants. Experiments were performed at 0, 2.5, 10, 50, 125, 250, and 500 nM, with each concentration being shown as a separate bar representing the averaged value of three experiments (with standard deviation), normalized to the activity of Hsp70 alone. **(e)** Fluorescence anisotropy measurements of DnaJA2 (blue), DnaJB1 (red), and DnaJB1$^{\Delta H5}$ (purple) binding to preformed α-synuclein fibrils. Data points represent the means of 3 independent measurements (with standard deviations), with the K_Ds for DnaJA2, DnaJB1, and DnaJB1$^{\Delta H5}$ being 1150 ± 170 nM, 780 ± 38 nM, and 730 ± 50 nM, respectively. **(f)** Fluorescence anisotropy measurements of DnaJB1 (red) and DnaJB1$^{\Delta H5}$ (purple) binding to Hsp70 T204 ATPase deficient mutant. Data points represent the means of 3 independent measurements (with standard deviations), with apparent K_Ds for DnaJB1, and DnaJB1$^{\Delta H5}$ being 10.6 ± 2.3 μM and 5.4 ± 1.4 μM, respectively. **(g)** Co-sedimentation assay assessing the recruitment of Hsp70 to preformed α-synuclein fibers by DnaJA2, DnaJB1, and DnaJB1$^{\Delta H5}$ chaperones. The assay was performed with 5 μM (1x) and 50 μM (10x) of indicated JDPs. Both DnaJB1 and DnaJB1$^{\Delta H5}$ efficiently recruit Hsp70 to the fibers, while DnaJA2, that has a single Hsp70 binding site per protomer, does not. The experiment was repeated twice with similar results. **(h)** Recruitment of Hsp70 to α-synuclein fibers by DnaJA2 (blue), DnaJB1 (red), and DnaJB1$^{\Delta H5}$ (purple) measured by fluorescence anisotropy. Data points represent the means of 3 independent measurements (with standard deviations). **(i)** Relative FRET efficiencies measured for wild-type Hsp70 or Hsp70$^{\Delta EEVD}$ incubated with α-synuclein fibers and in the presence of DnaJA2 (blue), DnaJB1 WT (red), or DnaJB1$^{\Delta H5}$ (purple). Data are presented as mean values ± s.e.m. of 3 independent measurements. In each experiment, half of the Hsp70 population was labeled with C494-AF488 (donor) and half with C494-AF584 (acceptor), and a FRET signal was observed when donor- and acceptor-labeled Hsp70s were in close proximity - indicating clustering.

References

1 Mayer, M. P. & Bukau, B. Hsp70 chaperones: cellular functions and molecular mechanism. *Cell Mol Life Sci* **62**, 670-684, doi:10.1007/s00018-004-4464-6 (2005).

2 Kampinga, H. H. & Craig, E. A. The HSP70 chaperone machinery: J proteins as drivers of functional specificity. *Nat Rev Mol Cell Biol* **11**, 579-592, doi:10.1038/nrm2941 (2010).

3 Rosenzweig, R., Nillegoda, N. B., Mayer, M. P. & Bukau, B. The Hsp70 chaperone network. *Nat Rev Mol Cell Biol*, doi:10.1038/s41580-019-0133-3 (2019).

4 Tiwari, S., Kumar, V., Jayaraj, G. G., Maiti, S. & Mapa, K. Unique structural modulation of a non-native substrate by cochaperone DnaJ. *Biochemistry* **52**, 1011-1018, doi:10.1021/bi301543g (2013).

5 Jiang, Y., Rossi, P. & Kalodimos, C. G. Structural basis for client recognition and activity of Hsp40 chaperones. *Science* **365**, 1313-1319, doi:10.1126/science.aax1280 (2019).

6 Tugarinov, V., Hwang, P. M., Ollerenshaw, J. E. & Kay, L. E. Cross-correlated relaxation enhanced 1H[bond]13C NMR spectroscopy of methyl groups in very high molecular weight proteins and protein complexes. *J Am Chem Soc* **125**, 10420-10428, doi:10.1021/ja030153x (2003).

7 Tugarinov, V., Kanelis, V. & Kay, L. E. Isotope labeling strategies for the study of high-molecular-weight proteins by solution NMR spectroscopy. *Nat Protoc* **1**, 749-754, doi:nprot.2006.101 [pii]10.1038/nprot.2006.101 (2006).

8 Kityk, R., Kopp, J. & Mayer, M. P. Molecular Mechanism of J-Domain-Triggered ATP Hydrolysis by Hsp70 Chaperones. *Mol Cell* **69**, 227-237 e224, doi:10.1016/j.molcel.2017.12.003 (2018).

9 Wentink, A., Nussbaum-Krammer, C. & Bukau, B. Modulation of Amyloid States by Molecular Chaperones. *Cold Spring Harb Perspect Biol* **11**, doi:10.1101/cshperspect.a033969 (2019).

10 Schilke, B. A. *et al.* Broadening the functionality of a J-protein/Hsp70 molecular chaperone system. *PLoS Genet* **13**, e1007084, doi:10.1371/journal.pgen.1007084 (2017).

11 Zarouchlioti, C., Parfitt, D. A., Li, W., Gittings, L. M. & Cheetham, M. E. DNAJ Proteins in neurodegeneration: essential and protective factors. *Philos Trans R Soc Lond B Biol Sci* **373**, doi:10.1098/rstb.2016.0534 (2018).

12 Gao, X. *et al.* Human Hsp70 Disaggregase Reverses Parkinson's-Linked alpha-Synuclein Amyloid Fibrils. *Mol Cell*, doi:10.1016/j.molcel.2015.07.012 (2015).

13 Rampelt, H. *et al.* Metazoan Hsp70 machines use Hsp110 to power protein disaggregation. *EMBO J* **31**, 4221-4235, doi:10.1038/emboj.2012.264 (2012).

14 Duennwald, M. L., Echeverria, A. & Shorter, J. Small heat shock proteins potentiate amyloid dissolution by protein disaggregases from yeast and humans. *PLoS Biol* **10**, e1001346, doi:10.1371/journal.pbio.1001346 (2012).

15 Scior, A. *et al.* Complete suppression of Htt fibrilization and disaggregation of Htt fibrils by a trimeric chaperone complex. *EMBO J* **37**, 282-299, doi:10.15252/embj.201797212 (2018).

16 Nachman E., W. A., Madiona K., Bousset L., Katsinelos T., Kampinga H., McEwan WA., R. Jahn RT., Melki R., Mogk A., Bukau B., and Nussbaum-Krammer C. Disassembly of Tau fibrils by the human Hsp70 disaggregation machinery generates small seeding-competent species *bioRxiv*, doi:http://dx.doi.org/10.1101/2019.12.16.876888 (2019).

17 Minami, Y., Hohfeld, J., Ohtsuka, K. & Hartl, F. U. Regulation of the heat-shock protein 70 reaction cycle by the mammalian DnaJ homolog, Hsp40. *J Biol Chem* **271**, 19617-19624, doi:10.1074/jbc.271.32.19617 (1996).

18 Karzai, A. W. & McMacken, R. A bipartite signaling mechanism involved in DnaJ-mediated activation of the Escherichia coli DnaK protein. *J Biol Chem* **271**, 11236-11246 (1996).

19 Yan, W. & Craig, E. A. The glycine-phenylalanine-rich region determines the specificity of the yeast Hsp40 Sis1. *Mol Cell Biol* **19**, 7751-7758 (1999).

20 Shen, Y. & Bax, A. Protein backbone and sidechain torsion angles predicted from NMR chemical shifts using artificial neural networks. *J Biomol NMR* **56**, 227-241, doi:10.1007/s10858-013-9741-y (2013).
21 Mesleh, M. F., Veglia, G., DeSilva, T. M., Marassi, F. M. & Opella, S. J. Dipolar waves as NMR maps of protein structure. *J Am Chem Soc* **124**, 4206-4207, doi:10.1021/ja0178665 (2002).
22 Qian, Y. Q., Patel, D., Hartl, F. U. & McColl, D. J. Nuclear magnetic resonance solution structure of the human Hsp40 (HDJ-1) J-domain. *J Mol Biol* **260**, 224-235, doi:10.1006/jmbi.1996.0394 (1996).
23 Yu, H. Y. *et al.* Roles of intramolecular and intermolecular interactions in functional regulation of the Hsp70 J-protein co-chaperone Sis1. *J Mol Biol* **427**, 1632-1643, doi:10.1016/j.jmb.2015.02.007 (2015).
24 Li, J., Wu, Y., Qian, X. & Sha, B. Crystal structure of yeast Sis1 peptide-binding fragment and Hsp70 Ssa1 C-terminal complex. *Biochem J* **398**, 353-360, doi:10.1042/BJ20060618 (2006).
25 Craig, E. A. & Marszalek, J. How Do J-Proteins Get Hsp70 to Do So Many Different Things? *Trends Biochem Sci* **42**, 355-368, doi:10.1016/j.tibs.2017.02.007 (2017).
26 Yu, H. Y., Ziegelhoffer, T. & Craig, E. A. Functionality of Class A and Class B J-protein co-chaperones with Hsp70. *FEBS Lett* **589**, 2825-2830, doi:10.1016/j.febslet.2015.07.040 (2015).
27 Battiste, J. L. & Wagner, G. Utilization of site-directed spin labeling and high-resolution heteronuclear nuclear magnetic resonance for global fold determination of large proteins with limited nuclear overhauser effect data. *Biochemistry* **39**, 5355-5365, doi:bi000060h [pii] (2000).
28 Clore, G. M. & Iwahara, J. Theory, practice, and applications of paramagnetic relaxation enhancement for the characterization of transient low-population states of biological macromolecules and their complexes. *Chem Rev* **109**, 4108-4139, doi:10.1021/cr900033p (2009).
29 Suzuki, H. *et al.* Peptide-binding sites as revealed by the crystal structures of the human Hsp40 Hdj1 C-terminal domain in complex with the octapeptide from human Hsp70. *Biochemistry* **49**, 8577-8584, doi:10.1021/bi100876n (2010).
30 Karamanos, T. K., Tugarinov, V. & Clore, G. M. Unraveling the structure and dynamics of the human DNAJB6b chaperone by NMR reveals insights into Hsp40-mediated proteostasis. *Proc Natl Acad Sci U S A* **116**, 21529-21538, doi:10.1073/pnas.1914999116 (2019).
31 Ruggieri, A. *et al.* Complete loss of the DNAJB6 G/F domain and novel missense mutations cause distal-onset DNAJB6 myopathy. *Acta neuropathologica communications* **3**, 44, doi:10.1186/s40478-015-0224-0 (2015).
32 Shen, Y. & Hendershot, L. M. ERdj3, a stress-inducible endoplasmic reticulum DnaJ homologue, serves as a cofactor for BiP's interactions with unfolded substrates. *Mol Biol Cell* **16**, 40-50, doi:10.1091/mbc.e04-05-0434 (2005).
33 Gelis, I. *et al.* Structural basis for signal-sequence recognition by the translocase motor SecA as determined by NMR. *Cell* **131**, 756-769, doi:S0092-8674(07)01269-X [pii]10.1016/j.cell.2007.09.039 (2007).
34 Gans, P. *et al.* Stereospecific isotopic labeling of methyl groups for NMR spectroscopic studies of high-molecular-weight proteins. *Angew Chem Int Ed Engl* **49**, 1958-1962, doi:10.1002/anie.200905660 (2010).
35 Delaglio, F. *et al.* NMRPipe: a multidimensional spectral processing system based on UNIX pipes. *J Biomol NMR* **6**, 277-293 (1995).
36 Kneller, T. D. G. a. D. G. *SPARKY 3*. (University of California).
37 Vranken, W. F. *et al.* The CCPN data model for NMR spectroscopy: development of a software pipeline. *Proteins* **59**, 687-696, doi:10.1002/prot.20449 (2005).
38 Karagoz, G. E. *et al.* N-terminal domain of human Hsp90 triggers binding to the cochaperone p23. *Proc Natl Acad Sci U S A* **108**, 580-585, doi:10.1073/pnas.1011867108 (2011).

39 Sekhar, A., Rosenzweig, R., Bouvignies, G. & Kay, L. E. Mapping the conformation of a client protein through the Hsp70 functional cycle. *Proc Natl Acad Sci U S A* **112**, 10395-10400, doi:10.1073/pnas.1508504112 (2015).
40 Constantine, K. L. *et al.* Aliphatic 1H and 13C resonance assignments for the 26-10 antibody VL domain derived from heteronuclear multidimensional NMR spectroscopy. *J Biomol NMR* **3**, 41-54 (1993).
41 Farrow, N. A. *et al.* Backbone dynamics of a free and phosphopeptide-complexed Src homology 2 domain studied by 15N NMR relaxation. *Biochemistry* **33**, 5984-6003 (1994).
42 Lyons, B. A., Tashiro, M., Cedergren, L., Nilsson, B. & Montelione, G. T. An improved strategy for determining resonance assignments for isotopically enriched proteins and its application to an engineered domain of staphylococcal protein A. *Biochemistry* **32**, 7839-7845 (1993).
43 Logan, T. M., Olejniczak, E. T., Xu, R. X. & Fesik, S. W. A general method for assigning NMR spectra of denatured proteins using 3D HC(CO)NH-TOCSY triple resonance experiments. *J Biomol NMR* **3**, 225-231 (1993).
44 Yamazaki, T., Formankay, J. D. & Kay, L. E. 2-Dimensional Nmr Experiments for Correlating C-13-Beta and H-1-Delta/Epsilon Chemical-Shifts of Aromatic Residues in C-13-Labeled Proteins Via Scalar Couplings. *Journal of the American Chemical Society* **115**, 11054-11055, doi:Doi 10.1021/Ja00076a099 (1993).
45 Tugarinov, V., Choy, W. Y., Orekhov, V. Y. & Kay, L. E. Solution NMR-derived global fold of a monomeric 82-kDa enzyme. *Proc Natl Acad Sci U S A* **102**, 622-627, doi:0407792102 [pii]10.1073/pnas.0407792102 (2005).
46 Zwahlen, C. *et al.* An NMR experiment for measuring methyl-methyl NOEs in C-13-labeled proteins with high resolution. *Journal of the American Chemical Society* **120**, 7617-7625, doi:Doi 10.1021/Ja981205z (1998).
47 Suzuki, H. *et al.* Peptide-Binding Sites As Revealed by the Crystal Structures of the Human Hsp40 Hdj1 C-Terminal Domain in Complex with the Octapeptide from Human Hsp70. *Biochemistry* **49**, 8577-8584, doi:10.1021/bi100876n (2010).
48 Lakomek, N. A., Ying, J. & Bax, A. Measurement of (1)(5)N relaxation rates in perdeuterated proteins by TROSY-based methods. *J Biomol NMR* **53**, 209-221, doi:10.1007/s10858-012-9626-5.
49 Mandel, A. M., Akke, M. & Palmer, A. G., 3rd. Backbone dynamics of Escherichia coli ribonuclease HI: correlations with structure and function in an active enzyme. *J Mol Biol* **246**, 144-163, doi:S0022283684700738 [pii] (1995).
50 W. H. Press, S. A. T., W. T. Vetterling, B. P. Flannery. *Numerical Recipes in C. The Art of Scientific Computing*. *Cambridge University Press* **Cambridge** (1999).
51 Ottiger, M., Delaglio, F. & Bax, A. Measurement of J and dipolar couplings from simplified two-dimensional NMR spectra. *J Magn Reson* **131**, 373-378, doi:10.1006/jmre.1998.1361 (1998).
52 Shen, Y. *et al.* Consistent blind protein structure generation from NMR chemical shift data. *Proc Natl Acad Sci U S A* **105**, 4685-4690, doi:10.1073/pnas.0800256105 (2008).
53 Shen, Y., Vernon, R., Baker, D. & Bax, A. De novo protein structure generation from incomplete chemical shift assignments. *J Biomol NMR* **43**, 63-78, doi:10.1007/s10858-008-9288-5 (2009).
54 Kuenze, G., Bonneau, R., Leman, J. K. & Meiler, J. Integrative Protein Modeling in RosettaNMR from Sparse Paramagnetic Restraints. *Structure*, doi:10.1016/j.str.2019.08.012 (2019).
55 Vernon, R., Shen, Y., Baker, D. & Lange, O. F. Improved chemical shift based fragment selection for CS-Rosetta using Rosetta3 fragment picker. *J Biomol NMR* **57**, 117-127, doi:10.1007/s10858-013-9772-4 (2013).

56 Shen, Y. & Bax, A. SPARTA+: a modest improvement in empirical NMR chemical shift prediction by means of an artificial neural network. *J Biomol NMR* **48**, 13-22, doi:10.1007/s10858-010-9433-9 (2010).
57 Bhattacharya, A., Tejero, R. & Montelione, G. T. Evaluating protein structures determined by structural genomics consortia. *Proteins* **66**, 778-795, doi:10.1002/prot.21165 (2007).
58 Laskowski, R. A., Rullmannn, J. A., MacArthur, M. W., Kaptein, R. & Thornton, J. M. AQUA and PROCHECK-NMR: programs for checking the quality of protein structures solved by NMR. *J Biomol NMR* **8**, 477-486, doi:10.1007/BF00228148 (1996).
59 Nillegoda, N. B. *et al.* Crucial HSP70 co-chaperone complex unlocks metazoan protein disaggregation. *Nature* **524**, 247-251, doi:10.1038/nature14884 (2015).
60 Tsai, J. & Douglas, M. G. A conserved HPD sequence of the J-domain is necessary for YDJ1 stimulation of Hsp70 ATPase activity at a site distinct from substrate binding. *J Biol Chem* **271**, 9347-9354 (1996).
61 Suh, W. C., Lu, C. Z. & Gross, C. A. Structural features required for the interaction of the Hsp70 molecular chaperone DnaK with its cochaperone DnaJ. *J Biol Chem* **274**, 30534-30539 (1999).

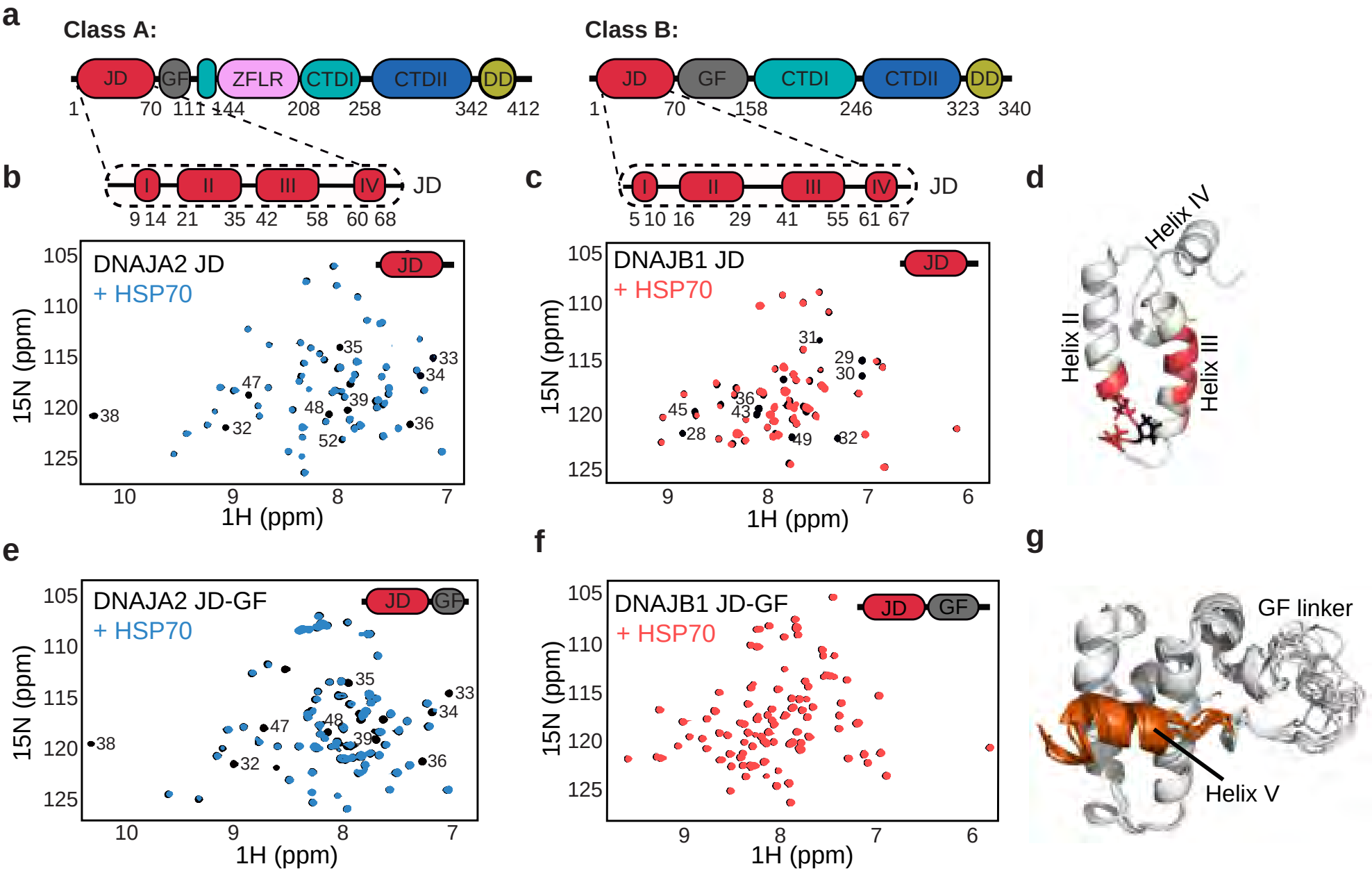
a
Class A:
JD
GF
ZFLR
CTDI
CTDII
DD
1
70
111
144
208
258
342
412
Class B:
JD
GF
CTDI
CTDII
DD
1
70
158
246
323
340
b
I
II
III
IV
JD
9 14 21 35 42 58 60 68
DNAJA2 JD
+ HSP70
JD
15N (ppm)
1H (ppm)
c
I
II
III
IV
JD
5 10 16 29 41 55 61 67
DNAJB1 JD
+ HSP70
JD
15N (ppm)
1H (ppm)
d
Helix IV
Helix II
Helix III
e
DNAJA2 JD-GF
+ HSP70
JD
GF
15N (ppm)
1H (ppm)
f
DNAJB1 JD-GF
+ HSP70
JD
GF
15N (ppm)
1H (ppm)
g
GF linker
Helix V

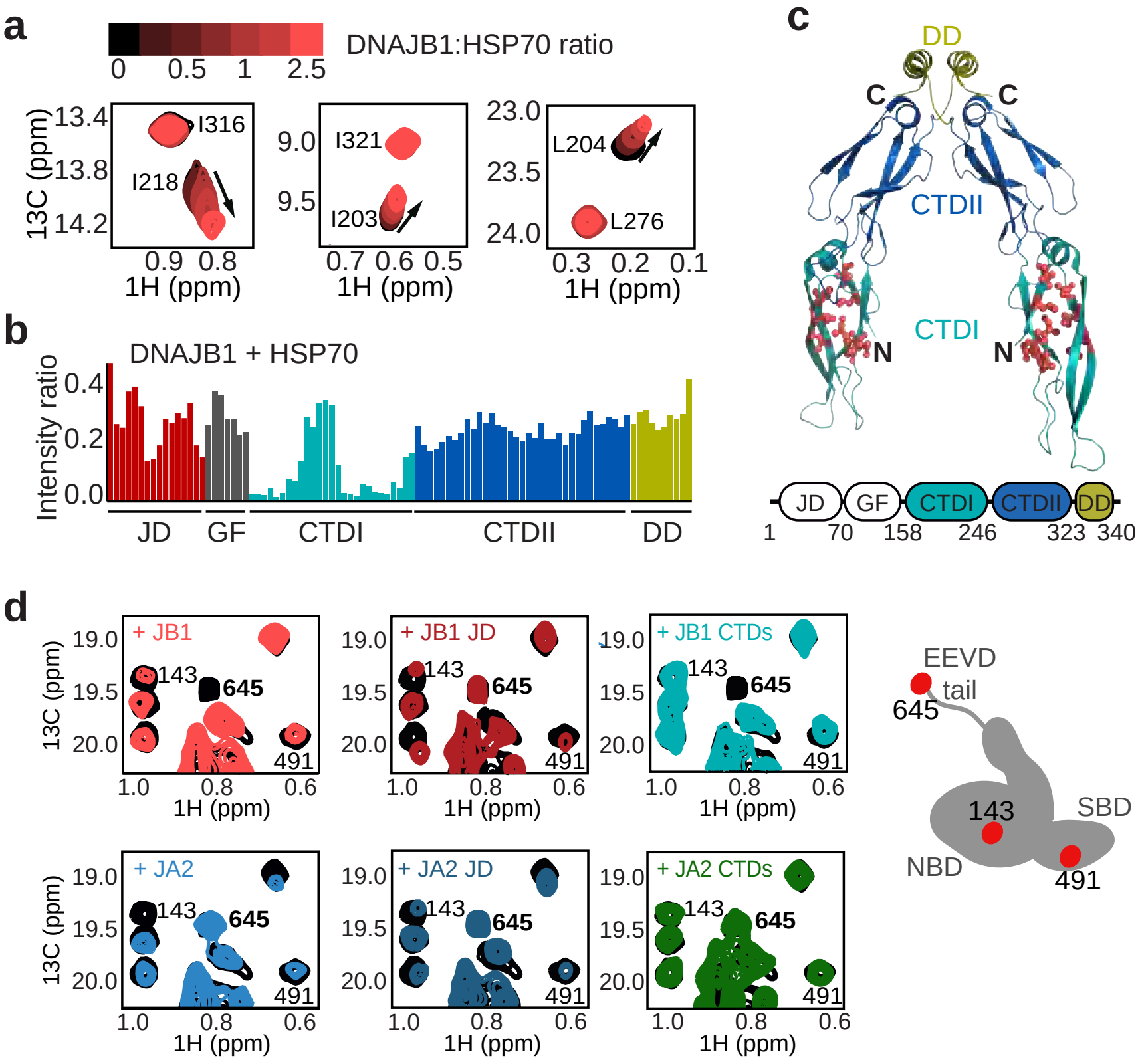
a
DNAJB1:HSP70 ratio
0
0.5
1
2.5
13C (ppm)
I316
I218
I321
I203
L204
L276
1H (ppm)
b
DNAJB1 + HSP70
Intensity ratio
JD
GF
CTDI
CTDII
DD
c
DD
C
C
CTDII
CTDI
N
N
1
70
158
246
323
340
d
+ JB1
+ JB1 JD
+ JB1 CTDs
+ JA2
+ JA2 JD
+ JA2 CTDs
143
645
491
EEVD
tail
SBD
NBD

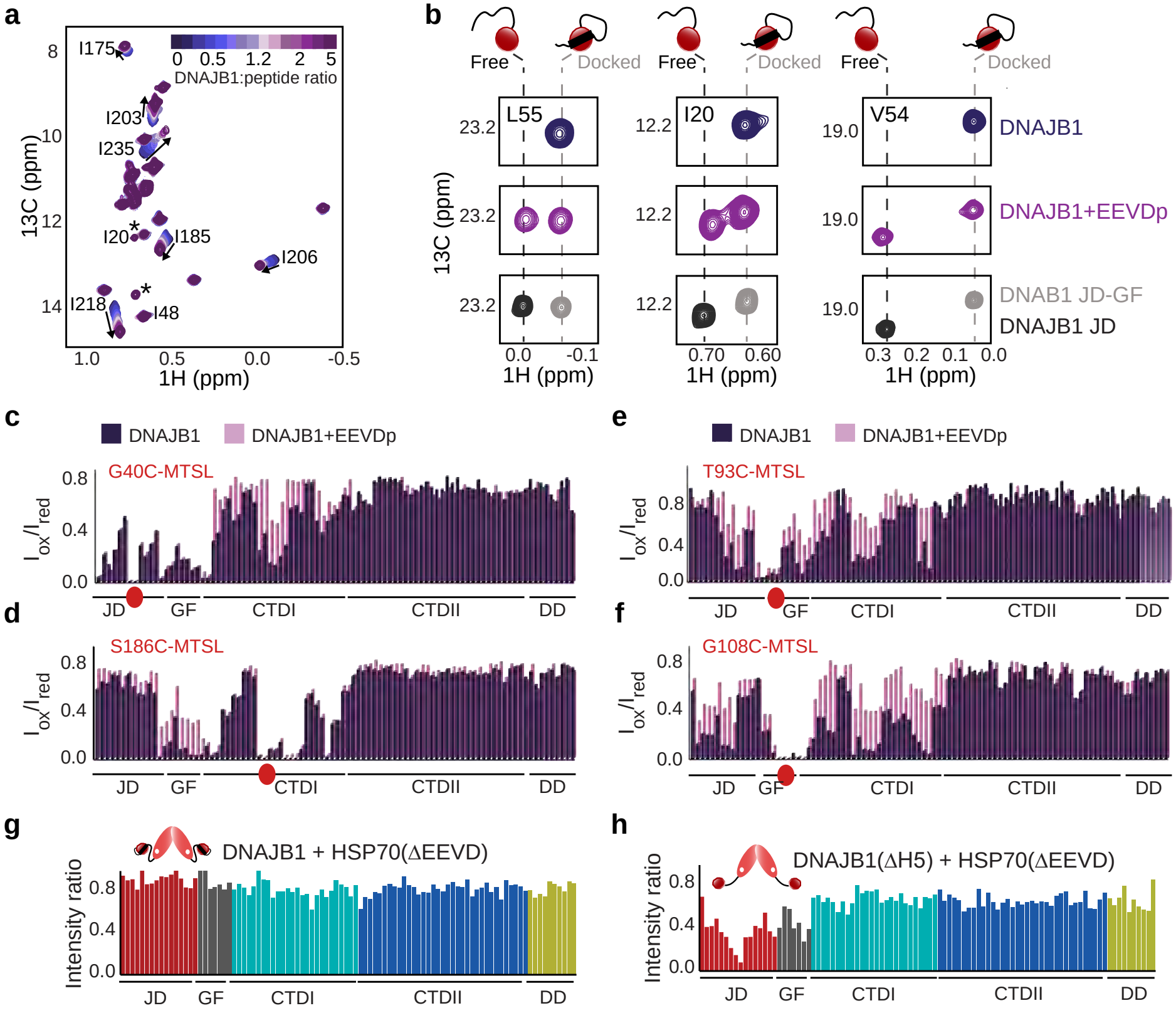
a
I175
I203
I235
I20
I185
I206
I218
I48
0 0.5 1.2 2 5
DNAJB1:peptide ratio
13C (ppm)
1H (ppm)
b
Free
Docked
L55
I20
V54
DNAJB1
DNAJB1+EEVDp
DNAB1 JD-GF
DNAJB1 JD
13C (ppm)
1H (ppm)
c
DNAJB1
DNAJB1+EEVDp
G40C-MTSL
e
T93C-MTSL
d
S186C-MTSL
f
G108C-MTSL
JD
GF
CTDI
CTDII
DD
g
DNAJB1 + HSP70(ΔEEVD)
h
DNAJB1(ΔH5) + HSP70(ΔEEVD)
Intensity ratio

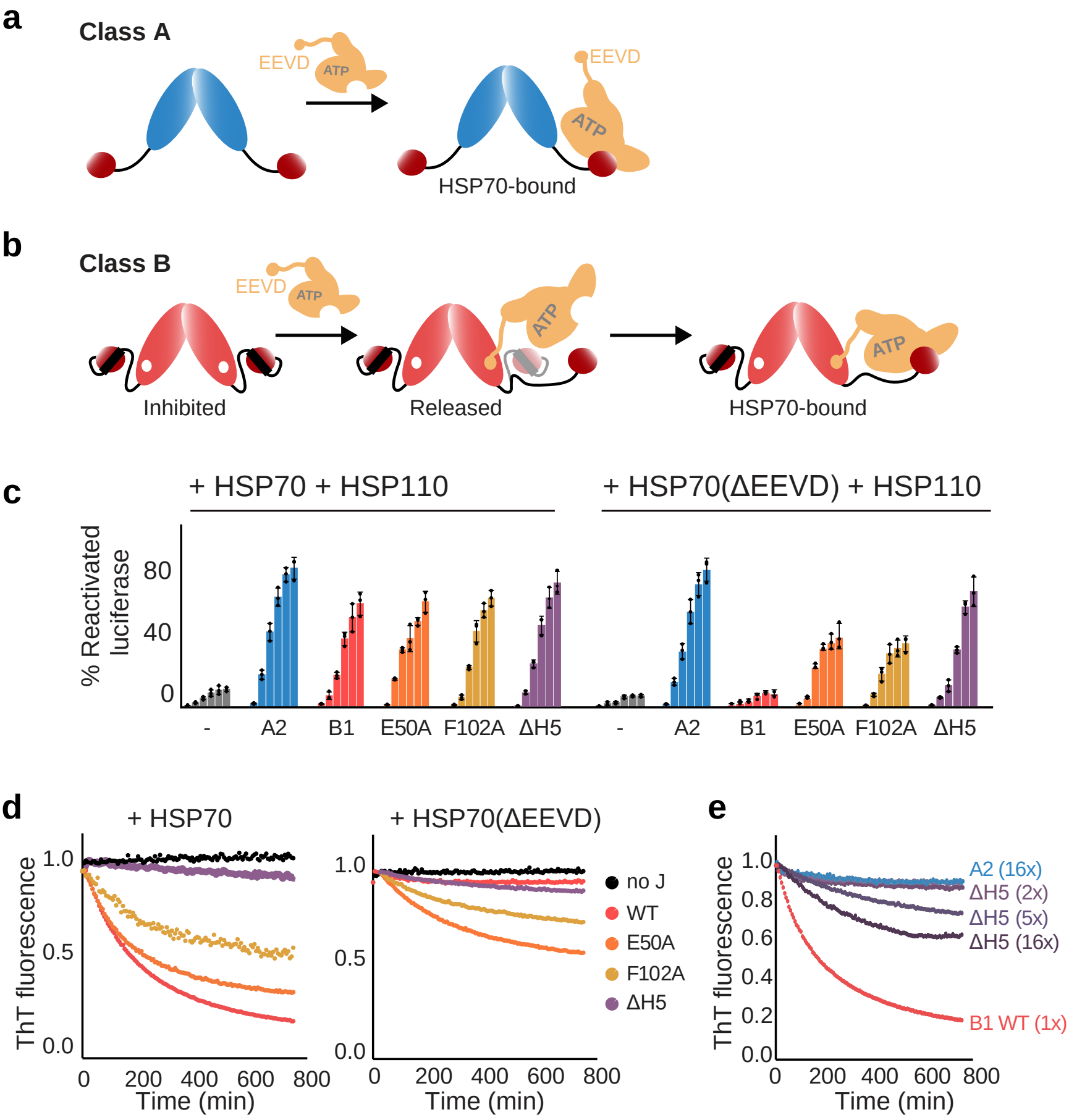
a
Class A
EEVD
ATP
EEVD
ATP
HSP70-bound
b
Class B
EEVD
ATP
ATP
ATP
Inhibited
Released
HSP70-bound
c
+ HSP70 + HSP110
+ HSP70(ΔEEVD) + HSP110
% Reactivated luciferase
80
40
0
-
A2
B1
E50A
F102A
ΔH5
-
A2
B1
E50A
F102A
ΔH5
d
+ HSP70
+ HSP70(ΔEEVD)
ThT fluorescence
1.0
0.5
0.0
0
200
400
600
800
Time (min)
no J
WT
E50A
F102A
ΔH5
e
ThT fluorescence
1.0
0.8
0.6
0.4
0.2
0.0
A2 (16x)
ΔH5 (2x)
ΔH5 (5x)
ΔH5 (16x)
B1 WT (1x)
Time (min)

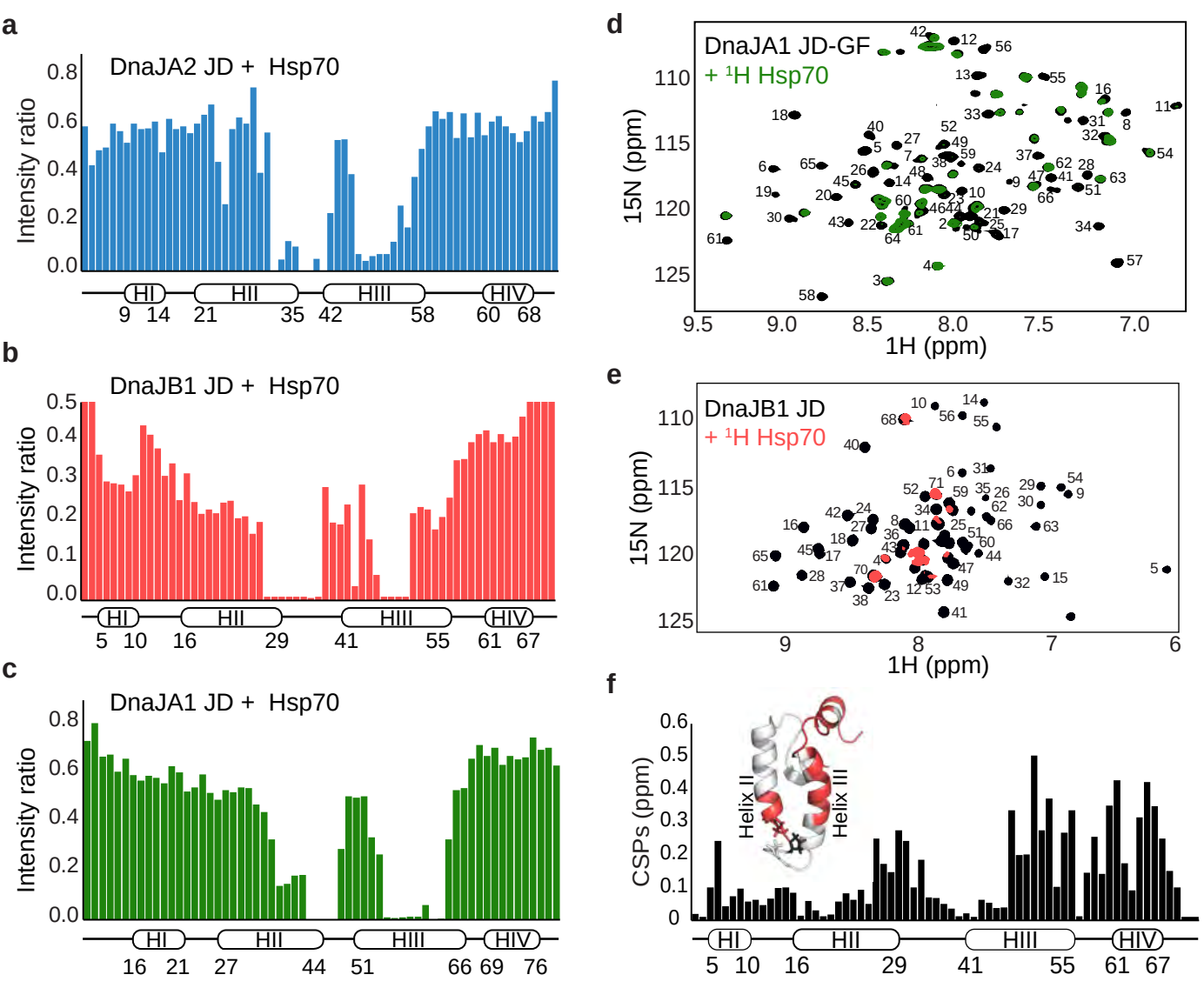

Extended Data Figure 1 | Interaction of JDP J-domains with Hsp70 chaperone.

(a-c) Residue-resolved NMR signal intensity ratios I/I_0, where I and I_0 are signal intensities for Hsp70-bound and free, DnaJA2^{JD} **(a)**, DnaJB1^{JD} **(b)**, and DnaJA1^{JD} **(c),** respectively. The positions of the four helices in each J-domain are indicated at the bottom of the plot. Large changes in intensity are detected at the end of helix II, the flexible loop containing the conserved HPD motif, and at helix III, corresponding to Hsp70-binding sites. In all three J-domains, similar residues are involved in binding, pointing to high conservation of JD-Hsp70 interaction. **(d)** Overlay of ^{1}H–^{15}N HSQC spectra of 0.2mM DnaJA1$^{JD\text{-}GF}$ alone (in black), and in the presence of two-fold excess of protonated (^{1}H) Hsp70 (green). Upon complex formation with Hsp70, the majority of the J-domain peaks were broadened out beyond detection, while the GF residues that are part of a flexible disordered linker were not affected, indicating that only the J-domain, and not the GF rich region, interacts with the Hsp70 chaperone. Assignments of J-domain residues are indicated on the spectrum. **(e)** ^{1}H–^{15}N HSQC spectra of 0.2mM DnaJB1^{JD} alone (in black), and in the presence of two-fold excess protonated (^{1}H) Hsp70 (red). Here too, addition of protonated Hsp70 causes severe peak broadening in the majority of the J-domain residues, with the exception of the flexible terminal residues and side chains. This, however, is in striking contrast to the spectrum of DnaJB1$^{JD\text{-}GF}$ under the same conditions (Fig. 1f of the main text), which showed no peak broadening, indicating lack of interaction with Hsp70. **(f)** Comparison of chemical shifts of residues 1-71 in the DnaJB1^{JD} and the same residues in the DnaJB1$^{JD\text{-}GF}$ construct. The differences in the chemical shift positions ($\Delta\delta$) are defined by the relation:

$\Delta\delta = \sqrt{(\Delta\delta_H)^2 + \left(\frac{\Delta\delta_N}{5}\right)^2}$, where, where $\Delta\delta_H$ and $\Delta\delta_N$ are ^{1}H proton and ^{15}N nitrogen shift changes between the chemical shifts of DnaJB1^{JD} and DnaJB1$^{JD\text{-}GF}$ residues (1-71). Large chemical shift changes are seen in residues of helix II and III, which are colored red on the structure of DnaJB1 J-domain. Residues displaying large differences between DnaJB1^{JD} and DnaJB1$^{JD\text{-}GF}$ are the same ones that show changes upon Hsp70 binding (helix II and III), and those in helix IV.

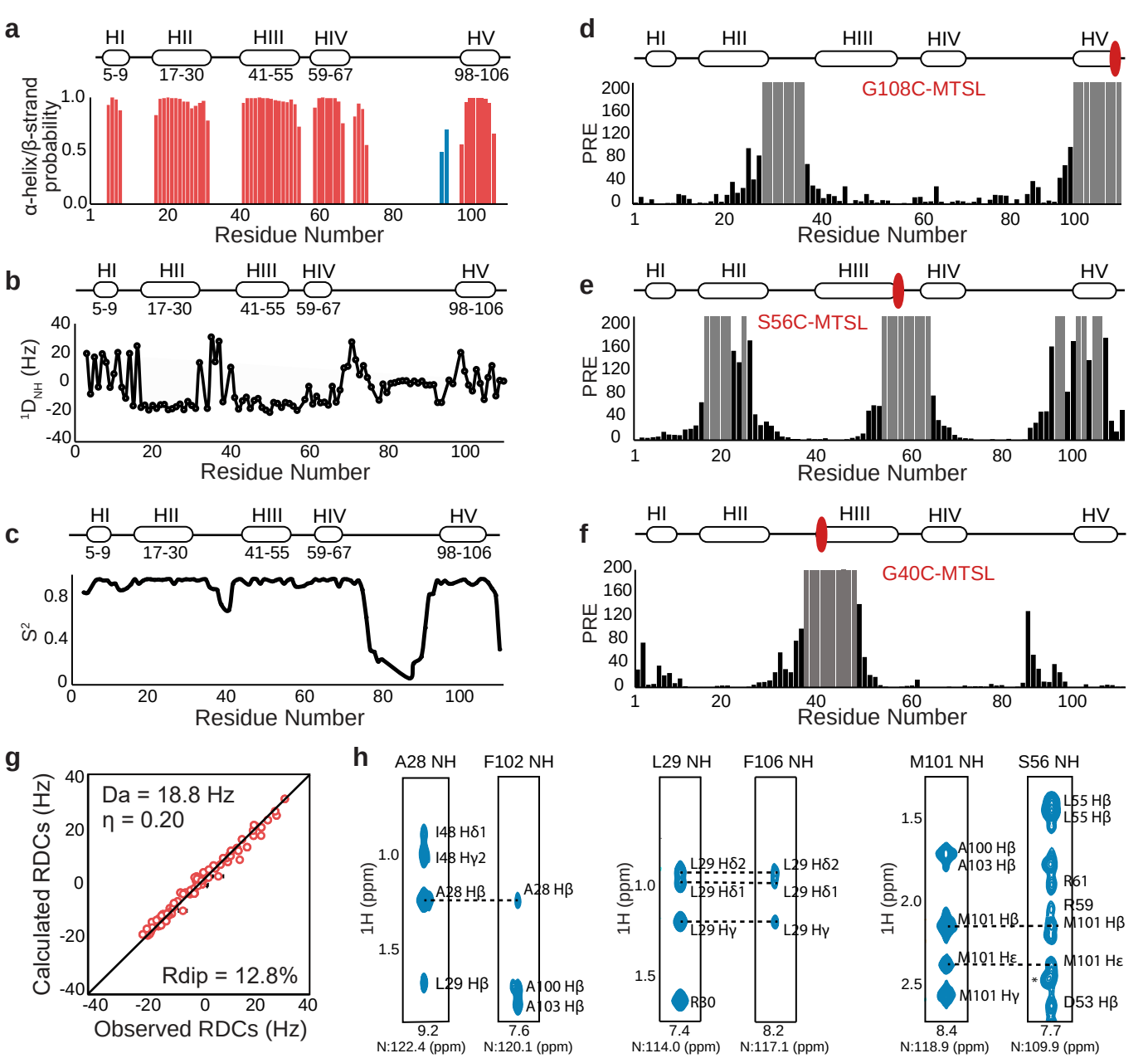

Extended Data Figure 2 | Structural characterization of DnaJB1$^{JD\text{-}GF}$

(a) TALOS$^+$ secondary structure probabilities[20] of DnaJB1$^{JD\text{-}GF}$ derived from backbone $^{13}C_\alpha$, $^{13}C_\beta$, $^{13}C'$, ^{15}N, and ^1H_N chemical shifts. Predicted α-helices are shown in red and β-sheets in blue. **(b)** Backbone order parameters (S^2) calculated using ModelFree[37] from ^{15}N relaxation data (see methods). The location of the five helices in DnaJB1$^{JD\text{-}GF}$ and their boundaries is indicated above the plot. **(c)** Backbone amide RDCs ($^1D_{NH}$) collected in 16 mg/mL phage pf1 alignment media. **(d-f)** ^1H_N PRE (R_2^{ox}-R_2^{red}) profiles recorded for nitroxide spin-labeled DnaJB1$^{JD\text{-}GF}$ with the MTSL spin-label located at residues 108 **(d)**, 56 **(e)**, and 40 **(f)**. ^1H-^{15}N cross-peaks that are broadened beyond detection in the oxidized state and were calculated to have a PRE ≥ 200 (see methods) are shown as grey bars. **(g)** Correlation between observed RDCs in pf1 alignment media and those calculated for the 10 lowest energy CS-ROSETTA structures. The RDC R-factor, Rdip, is given by:

$R_{dip} = \{\langle (D_{obs} - D_{cal})^2 \rangle / (2\langle D_{obs}^2 \rangle)\}^{1/2}$, where D_{obs} and D_{cal} are the observed and calculated RDC values, respectively. Da and η are the magnitude (normalized to the N-H RDCs) and rhombicity, respectively, of the alignment tensor. **(h)** Select strips from a 3D NOESY-HSQC experiment depicting long range methyl-NH NOEs for residues 28-102 (left), 29-106 (middle), and 101-56 (right), and indicating long range interactions between helix V and helices II and III.

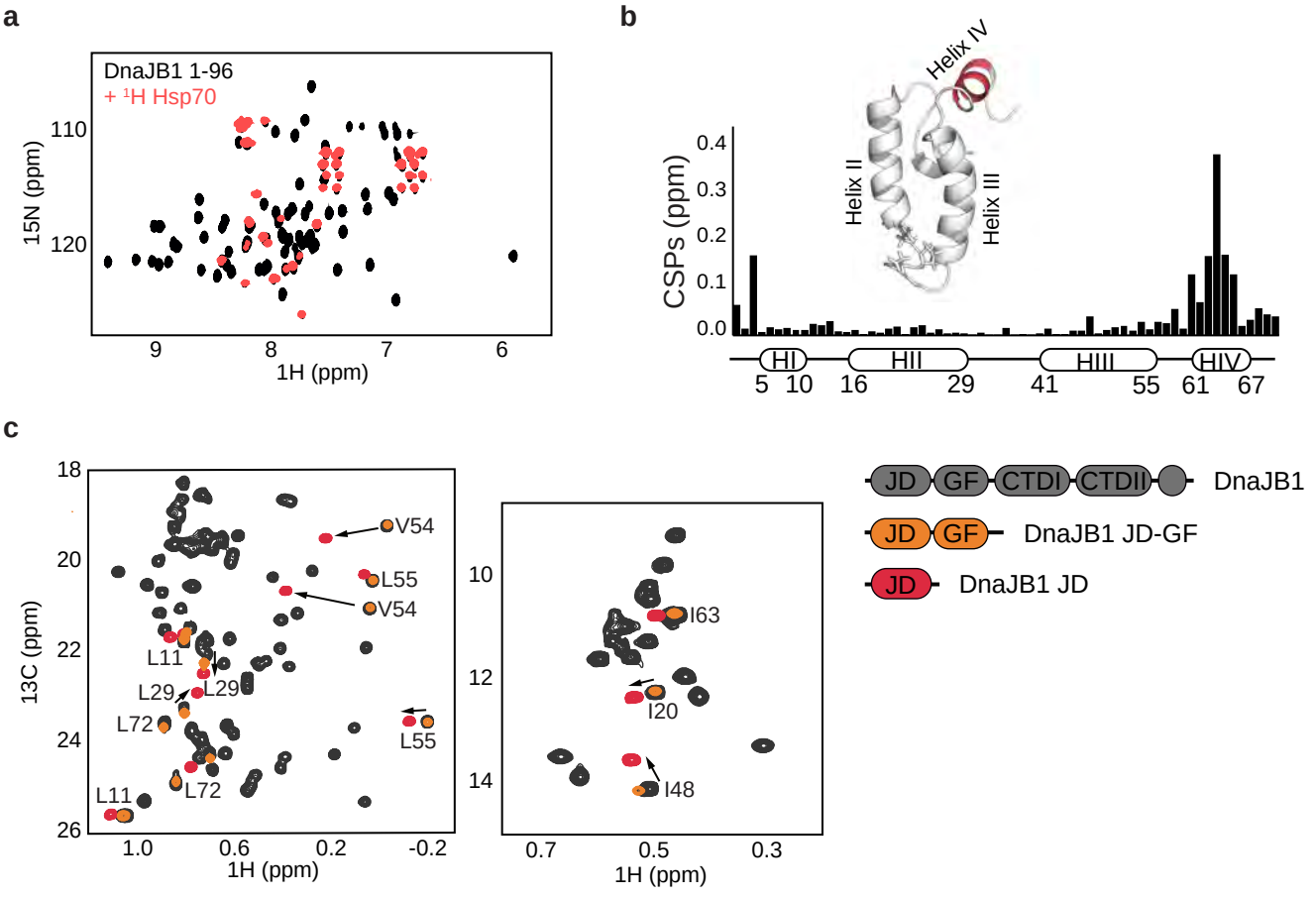

Extended Data Figure 3 | Deletion of helix V removes the GF inhibition of the J-domain and restores Hsp70 binding

(a) Overlay of ^{1}H-^{15}N HSQC correlation maps of 0.2mM DnaJB1$^{1-96}$ alone (black), and in complex with 0.2mM Hsp70 (red). Deletion of helix V residues restores the ability of DnaJB1 J-domain to interact with Hsp70, even in the presence of the GF region. **(b)** Differences in chemical shifts between DnaJB1^{JD} (res 1-71) and DnaJB1$^{1-96}$ construct lacking helix V. No significant changes in the spectra were observed between the two constructs, with the exception of residues located in helix IV (colored red on the structure of DnaJB1 J-domain), which connects the JD and GF. **(c)** ^{1}H–^{13}C HMQC spectra showing the leucine\valine (left) and isoleucine (right) regions of 0.2mM $^{13}CH_3$-ILVM labeled full-length DnaJB1 (grey), DnaJB1^{JD} (red), and DnaJB1$^{JD\text{-}GF}$ (orange). The DnaJB1$^{JD\text{-}GF}$ peaks overlap with those of full length DnaJB1 (with the exception of small CSPs observed for residues 29 and 48), while those of free JD do not, indicating that in the full length protein the J-domain is in the GF-inhibited conformation.

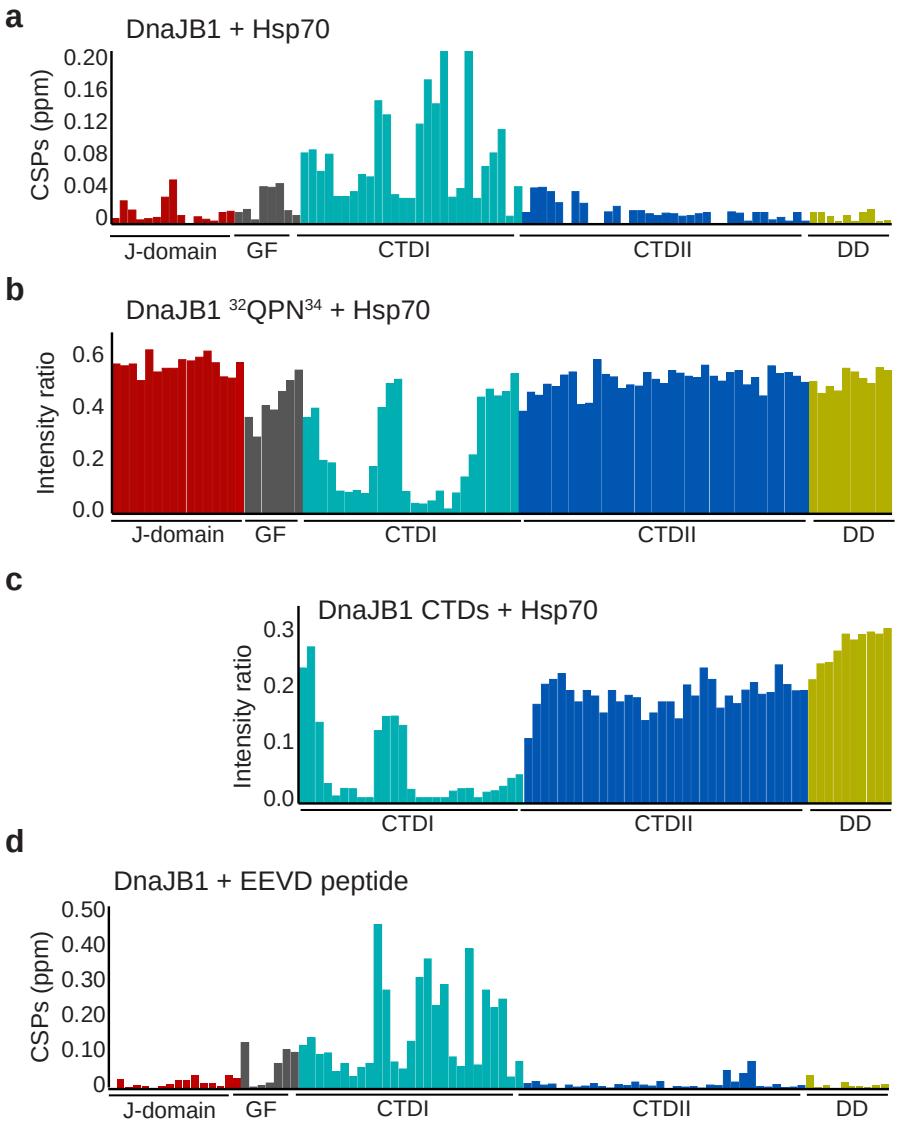

Extended Data Figure 4 | Interaction of DnaJB1 with Hsp70

(a) Chemical shift perturbations induced by Hsp70 binding to [^{2}H, $^{13}CH_3$-ILVM]-labelled DnaJB1. CSPs are defined by the relation $\Delta\delta = \sqrt{\left(\frac{\Delta\delta_H}{\alpha}\right)^2 + \left(\frac{\Delta\delta_C}{\beta}\right)^2}$, where $\Delta\delta_H$ and $\Delta\delta_C$ are methyl ^{1}H and ^{13}C chemical shift changes between apo and bound forms of the protein, and α (β) is one standard deviation from the methyl ^{1}H (^{13}C) chemical shifts deposited in the Biological Magnetic Resonance Data Bank (α is 0.29 (I), 0.28 (L), 0.27 (V) and 0.41 (M), whereas β is 1.65 (I), 1.6 (L), 1.4 (V), and 1.54 (M)). While Hsp70 binds to two sites in DnaJB1 (J-domain and CTDI), large chemical shifts changes are observed only in CTDI, indicating that this domain binds to Hsp70 in a transient manner (on a fast NMR time scale). **(b)** Per-residue peak intensity ratios of DnaJB1^{32QPN34}, in the absence, and presence of Hsp70 chaperone. In this variant, conserved residues (32-34) in the J-domain HPD motif, which is essential for Hsp70 activation, were mutated to QPN. Upon addition of Hsp70, no changes in intensities were detected for the J-domain residues, indicating that, as expected, mutations to the HPD motif abolish the J-domain-Hsp70 interaction[38,39]. The DnaJB1 CTDI interaction with Hsp70, however, remained strong and was unaffected by the mutation. **(c)** Peak intensity ratios of DnaJB1 CTDs (res 154-340) alone, and in complex with Hsp70 chaperone. The interaction of Hsp70 with the CTDI of DnaJB1 occurs independently of the JD. **(d)** Differences in chemical shifts between free DnaJB1 and DnaJB1 in complex with a synthetic peptide corresponding to the last 20 amino acids of the Hsp70 C-terminal tail. Large chemical shift perturbations are detected in the CTDI region of DnaJB1, similar to those observed upon DnaJB1 binding to full length Hsp70 (see panel a).

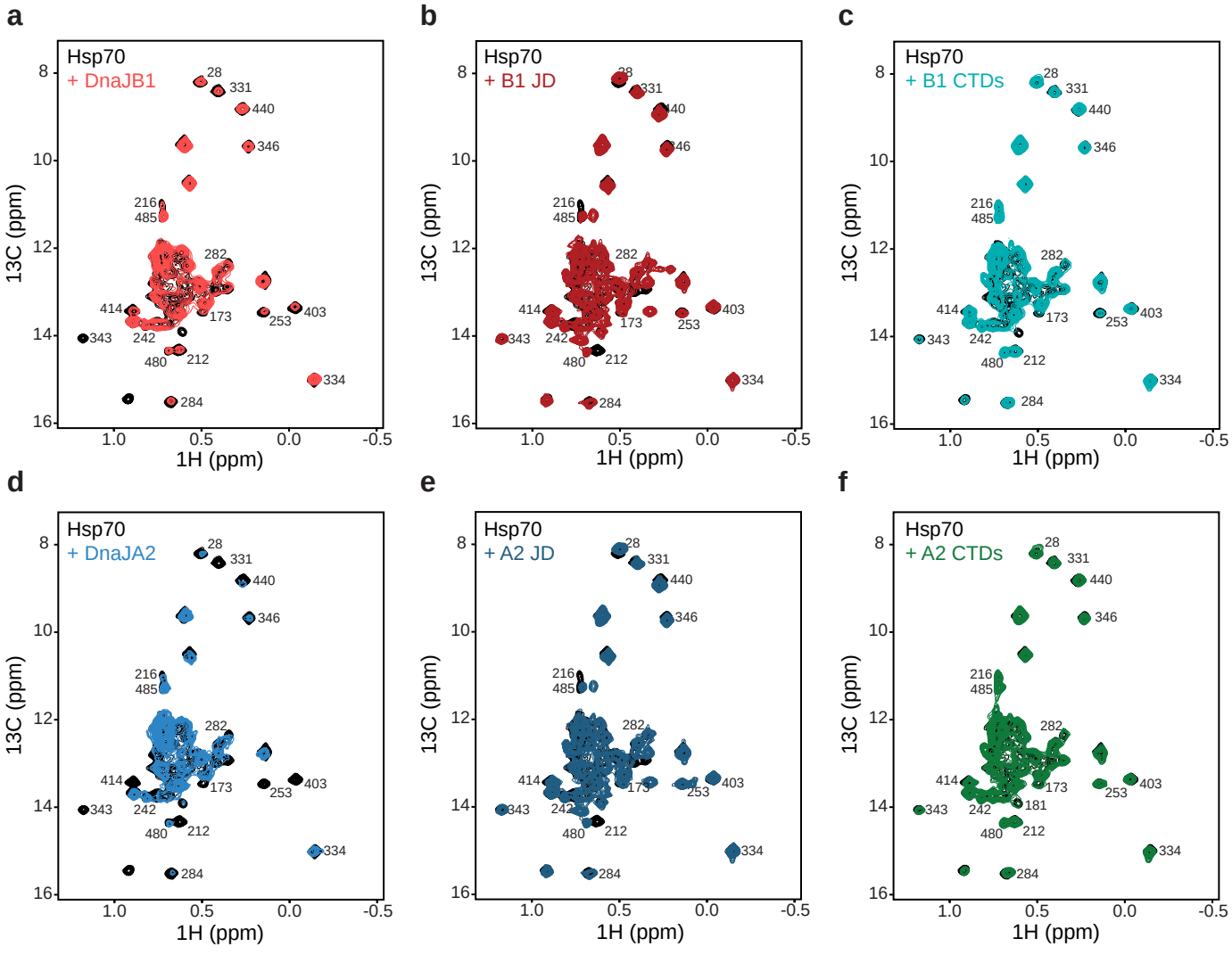

Extended Data Figure 5 | Hsp70 binds to the CTDI of DnaJB1 but not of DnaJA2

Overlay of ^{1}H-^{13}C HMQC correlation maps of ILVM-labeled Hsp70 (black) and Hsp70 in complex with DnaJB1 **(a,** light red**)**, DnaJB1 J-domain **(b,** dark red**),** and DnaJB1 CTDs **(c,** cyan**)**. DnaJB1 J-domain interacts with residues in Hsp70 NBD and SBD, similarly to the interaction observed between *E.coli* DnaK and DnaJ J-domain. DnaJB1 CTDs, however, interact with a different region of Hsp70, corresponding to the disordered C-terminal tail of Hsp70. Interaction of ILVM-labeled Hsp70 with DnaJA2 **(d,** light blue**)**, DnaJA2 J-domain **(e,** dark blue**)**, and DnaJA2 CTDs **(f,** green**)**. The residues of DnaJA2 J-domain interact with similar Hsp70 residues as DnaJB1 J-domain, in both cases located at the interface between NBD and SBD. Unlike DnaJB1, however, no interaction was observed between DnaJA2 CTDs and Hsp70.

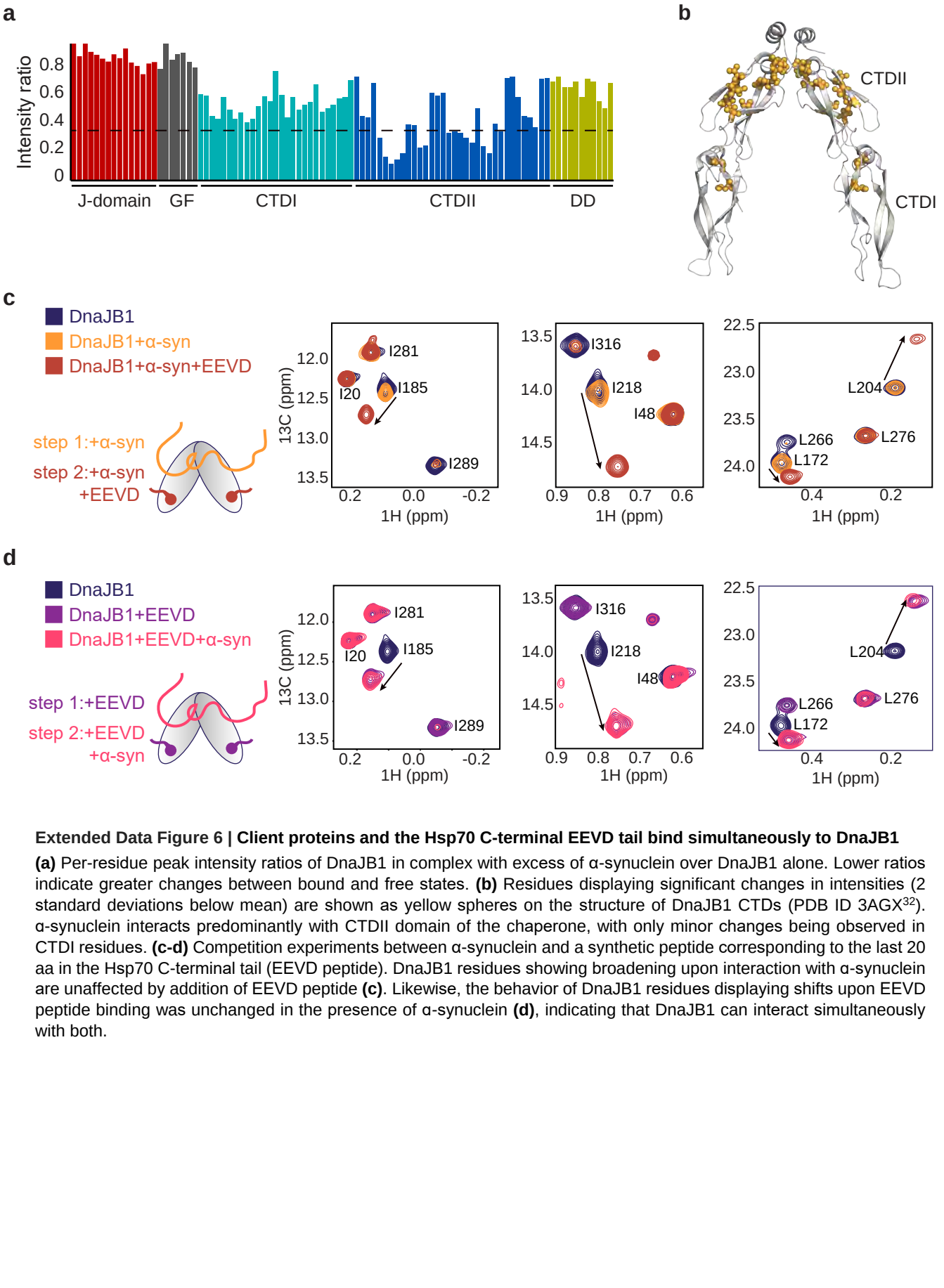

Extended Data Figure 6 | Client proteins and the Hsp70 C-terminal EEVD tail bind simultaneously to DnaJB1

(a) Per-residue peak intensity ratios of DnaJB1 in complex with excess of α-synuclein over DnaJB1 alone. Lower ratios indicate greater changes between bound and free states. **(b)** Residues displaying significant changes in intensities (2 standard deviations below mean) are shown as yellow spheres on the structure of DnaJB1 CTDs (PDB ID 3AGX[32]). α-synuclein interacts predominantly with CTDII domain of the chaperone, with only minor changes being observed in CTDI residues. **(c-d)** Competition experiments between α-synuclein and a synthetic peptide corresponding to the last 20 aa in the Hsp70 C-terminal tail (EEVD peptide). DnaJB1 residues showing broadening upon interaction with α-synuclein are unaffected by addition of EEVD peptide **(c)**. Likewise, the behavior of DnaJB1 residues displaying shifts upon EEVD peptide binding was unchanged in the presence of α-synuclein **(d)**, indicating that DnaJB1 can interact simultaneously with both.

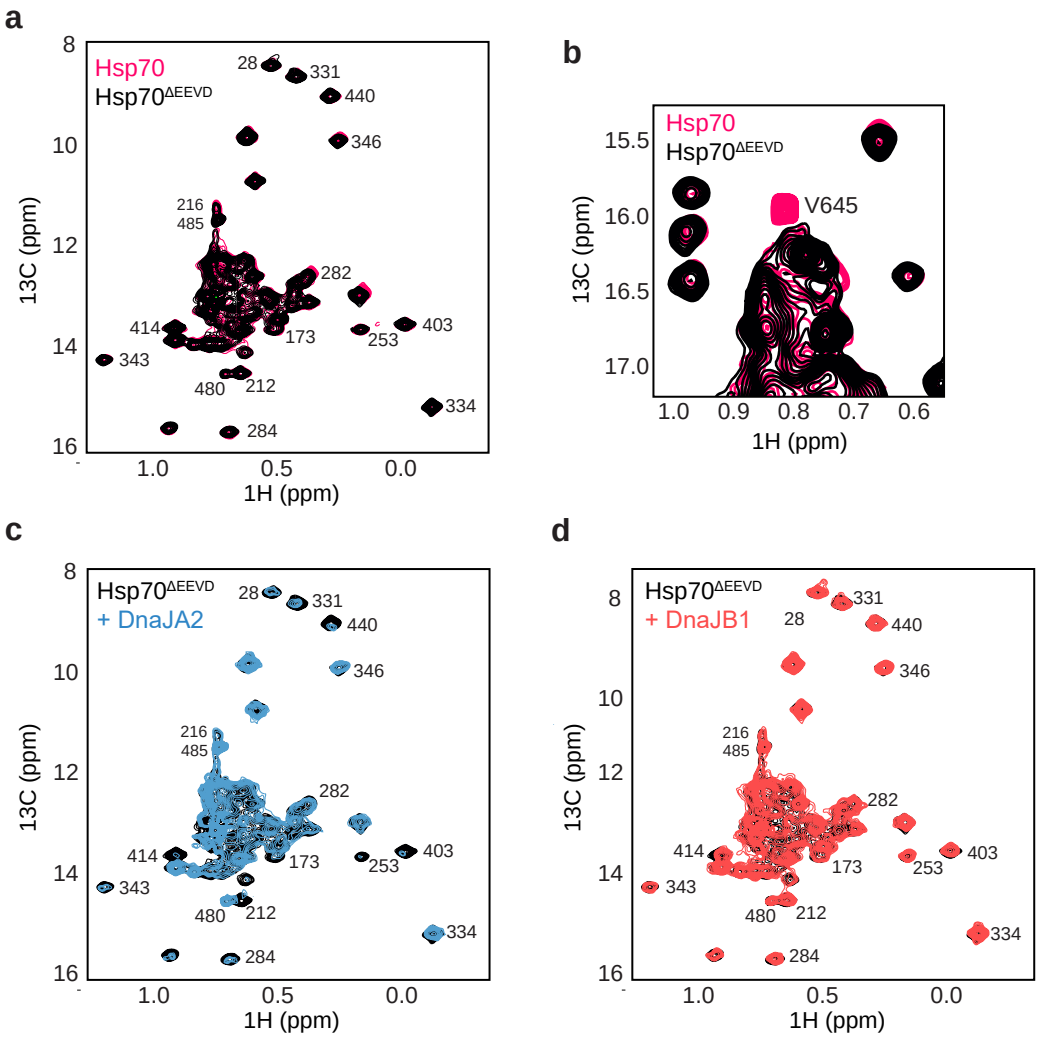

Extended Data Figure 7 | Removal of the Hsp70 EEVD tail abolishes binding to class B JDPs

(a) ^{1}H-^{13}C HMQC spectra of Hsp70 (pink) and Hsp70$^{\Delta EEVD}$ (black) showing the isoleucine **(a)** and valine **(b)** spectral regions. No conformational changes were detected in the Hsp70 chaperone upon deletion of the four C-terminal residues (EEVD). The only visible difference between the two spectra is the lack of the V645 peak in **(b)**, as this residue is part of the C-terminal tail that was deleted in Hsp70$^{\Delta EEVD}$. **(c,d)** Interaction of Hsp70$^{\Delta EEVD}$ with DnaJA2 **(c)** and DnaJB1 **(d)**. The interaction between DnaJA2 and Hsp70$^{\Delta EEVD}$ occurs via the same residues as between DnaJA2 and wt Hsp70 (**c**, blue; compare to Extended Data Figure 5c), while no interaction was detected between Hsp70$^{\Delta EEVD}$ and DnaJB1 (**d**, red).

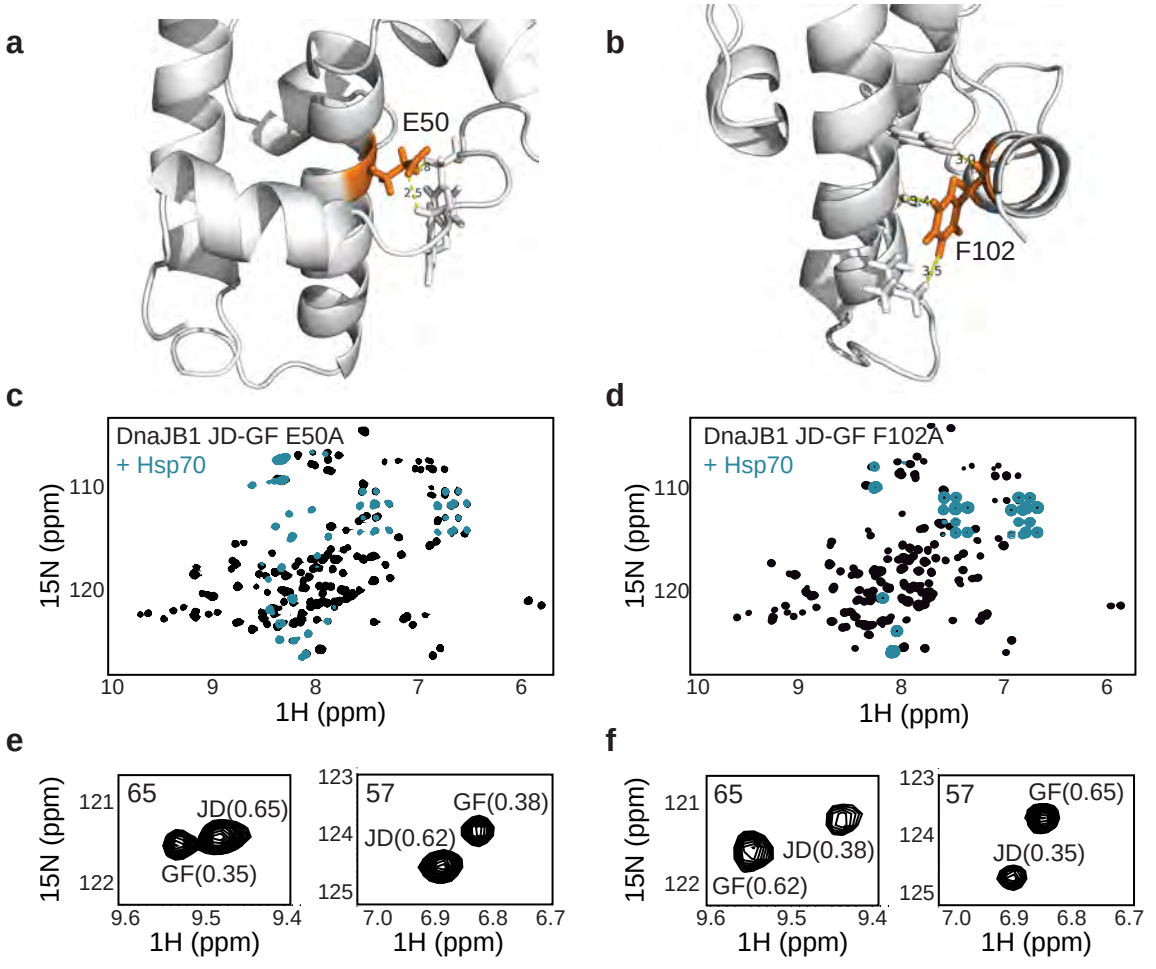

Extended Data Figure 8 | DnaJB1 mutants with released GF inhibition of the JD

(a-b) Cartoon representation of DnaJB1$^{JD\text{-}GF}$, highlighting the position of residues E50 **(a)** and F102 **(b)** that were mutated to alanines to generate DnaJB1$^{JD\text{-}GF}$ constructs with a released J-domain. **(c-d)** ^{1}H-^{15}N HSQC spectra of DnaJB1$^{JD\text{-}GF}$ E50A **(c)** and DnaJB1$^{JD\text{-}GF}$ F102A **(d)** alone, and in complex with Hsp70 (teal). While wt DnaJB1$^{JD\text{-}GF}$ was unable to bind Hsp70, partial release of the J-domain by targeted mutation in either the J-domain or GF region generates DnaJB1$^{JD\text{-}GF}$ constructs that bind Hsp70 with high affinity - as indicated by the severe broadening of the peaks in the bound spectrum. **(e-f)** Selected regions of the HSQC spectra showing residues D57 and D65 of DnaJB1$^{JD\text{-}GF}$ E50A **(e)** and F102A **(f)** in slow exchange between the GF-inhibited and released J-domain conformations. The population of each conformation was calculated by integrating the peak volumes, and is indicated for each residue. Overall, E50A mutation to the J-domain releases 64% while F102A mutation to the GF helix V releases 36%.

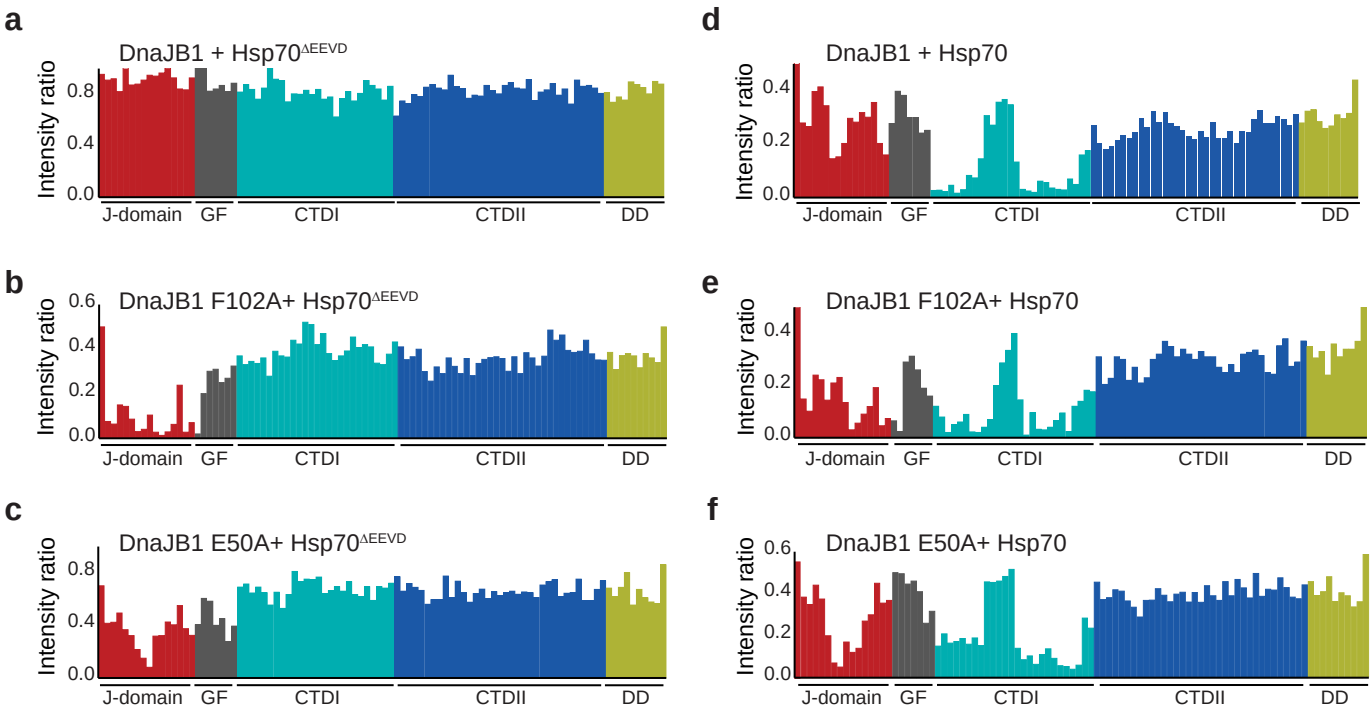

Extended Data Figure 9 | DnaJB1 mutants with partially released JD can interact with Hsp70 lacking the C-terminal tail.

(a-c) Peak intensity ratios of DnaJB1 WT **(a)**, DnaJB1 F102A **(b)**, and DnaJB1 E50A **(c)** in the presence of 2-fold molar excess of Hsp70$^{\Delta EEVD}$ chaperone lacking the four last residues (EEVD) of the C-terminal tail. All plots are normalized, per residue, by the peak intensities of each of the DnaJB1 variants alone. WT DnaJB1 protein is unable to bind to Hsp70$^{\Delta EEVD}$, as Hsp70 C-terminal is required for the release of its J-domain. However, both DnaJB1 mutants with partially released JDs bound to Hsp70, though the interaction was only through their J-domain, as the presence of Hsp70 C-terminal tail is required for binding of DnaJB1 CTDI **(d-e)**.

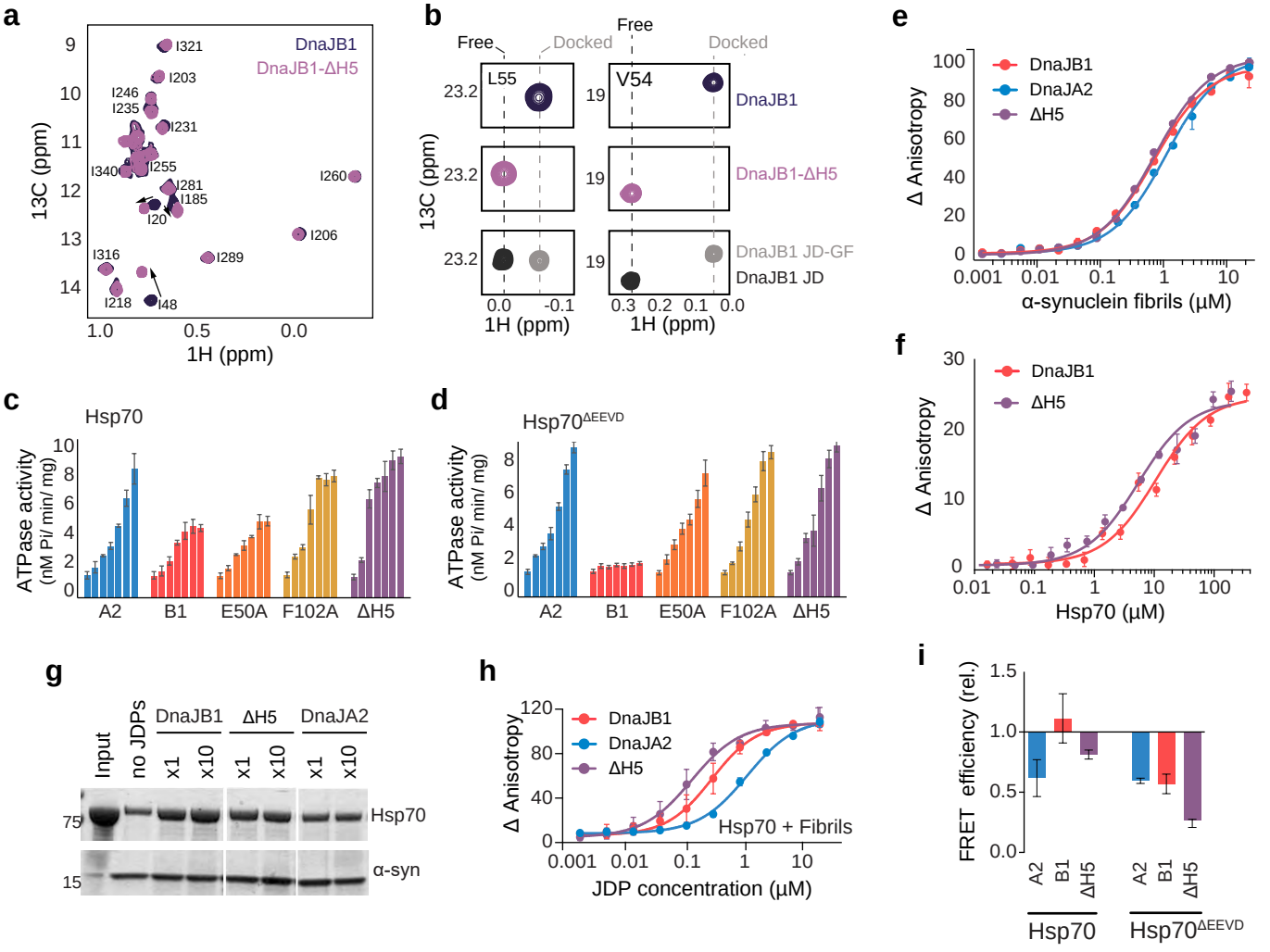

Extended Data Figure 10 | Characterization of Hsp70 activity with constitutively JD-released (DnaJB1$^{\Delta H5}$) mutant

(a) Spectrum of DnaJB1$^{\Delta H5}$ mutant (purple), containing a released J-domain, overlayed onto the spectrum of WT DnaJB1(blue). Outside of the J-domain residues, no changes were observed to the overall conformation of the chaperone. **(b)** DnaJB1 J-domain residues L55 and V54 display different chemical shifts in the GF-inhibited (gray), and free J-domain (black) conformations. J-domain of DnaJB1$^{\Delta H5}$ mutant is shown to be fully released. **(c-d)** Steady-state ATPase activity of 250 nM Hsp70 **(c)** or Hsp70$^{\Delta EEVD}$ **(d)** chaperone measured in the presence of increasing concentrations of DnaJA2 (blue), DnaJB1 WT (red), DnaJB1^{E50A} (orange), DaJB1^{F102A} (yellow), or DnaJB1$^{\Delta H5}$ (purple) variants. Experiments were performed at 0, 2.5, 10, 50, 125, 250, and 500 nM, with each concentration being shown as a separate bar representing the averaged value of three experiments (with standard deviation), normalized to the activity of Hsp70 alone. **(e)** Fluorescence anisotropy measurements of DnaJA2 (blue), DnaJB1 (red), and DnaJB1$^{\Delta H5}$ (purple) binding to preformed α-synuclein fibrils. Data points represent the means of 3 independent measurements (with standard deviations), with the K_Ds for DnaJA2, DnaJB1, and DnaJB1$^{\Delta H5}$ being 1150 ± 170 nM, 780 ± 38 nM, and 730 ± 50 nM, respectively. **(f)** Fluorescence anisotropy measurements of DnaJB1 (red) and DnaJB1$^{\Delta H5}$ (purple) binding to Hsp70 T204 ATPase deficient mutant. Data points represent the means of 3 independent measurements (with standard deviations), with apparent K_Ds for DnaJB1, and DnaJB1$^{\Delta H5}$ being 10.6 ± 2.3 μM and 5.4 ± 1.4 μM, respectively. **(g)** Co-sedimentation assay assessing the recruitment of Hsp70 to preformed α-synuclein fibers by DnaJA2, DnaJB1, and DnaJB1$^{\Delta H5}$ chaperones. The experiment was performed with 5 μM (1x) and 50 μM (10x) of indicated JDPs. Both DnaJB1 and DnaJB1$^{\Delta H5}$ efficiently recruit Hsp70 to the fibers, while DnaJA2, that has a single Hsp70 binding site per protomer, does not. **(h)** Recruitment of Hsp70 to α-synuclein fibers by DnaJA2 (blue), DnaJB1 (red), and DnaJB1$^{\Delta H5}$ (purple) measured by fluorescence anisotropy. **(i)** Relative FRET efficiencies measured for wild-type Hsp70 or Hsp70$^{\Delta EEVD}$ incubated with α-synuclein fibers and in the presence of DnaJA2 (blue), DnaJB1 WT (red), and DnaJB1$^{\Delta H5}$ (purple). In each experiment, half of the Hsp70 population was labeled with C494-AF488 (donor) and half with C494-AF584 (acceptor), and FRET signal was observed when donor- and acceptor-labeled Hsp70s were in close proximity - indicating clustering. Only the combination of WT DnaJB1 and WT Hsp70 shows significant clustering of the fibrils.

References

20 Shen, Y. & Bax, A. Protein backbone and sidechain torsion angles predicted from NMR chemical shifts using artificial neural networks. *J Biomol NMR* **56**, 227-241, doi:10.1007/s10858-013-9741-y (2013).

32 Suzuki, H. *et al.* Peptide-binding sites as revealed by the crystal structures of the human Hsp40 Hdj1 C-terminal domain in complex with the octapeptide from human Hsp70. *Biochemistry* **49**, 8577-8584, doi:10.1021/bi100876n (2010).

37 Mandel, A. M., Akke, M. & Palmer, A. G., 3rd. Backbone dynamics of Escherichia coli ribonuclease HI: correlations with structure and function in an active enzyme. *J Mol Biol* **246**, 144-163, doi:S0022283684700738 [pii] (1995).

38 Tsai, J. & Douglas, M. G. A conserved HPD sequence of the J-domain is necessary for YDJ1 stimulation of Hsp70 ATPase activity at a site distinct from substrate binding. *J Biol Chem* **271**, 9347-9354 (1996).

39 Suh, W. C., Lu, C. Z. & Gross, C. A. Structural features required for the interaction of the Hsp70 molecular chaperone DnaK with its cochaperone DnaJ. *J Biol Chem* **274**, 30534-30539 (1999).

Supplementary Table 1 | NMR and refinement statistics for DNAJB1$^{JD\text{-}GF}$

	DNAJB1 chaperone residues 1-111 (PDB 6Z5N)
NMR distance and dihedral constraints	
Distance constraints	
Total NOE	1271
Short range ($\|i-j\|<2$)	469
Medium-range ($\|i-j\|\leq 4$)	298
Long-range ($\|i-j\|>4$)	504
^{1}HN-Γ_2 PRE restraints	88
Total dihedral angle restraints	
ϕ	80
ψ	80
$^{1}D_{NH}$ RDC restraints	
PEG/hexanol alignment medium	95
pf1 alignment medium[a]	95
Structure statistics[b]	
Violations (mean and s.d.)	
Distance constraints (Å)	0.15±0.02
Max. distance constraint violation (Å)	0.9
Deviations from idealized geometry	
Bond lengths (Å)	0.01
Bond angles (°)	0.4
Q-factor (%)	10.9±0.6
Average pairwise r.m.s. deviation[c] (Å)	
Heavy	1.0
Backbone	0.5
Ramachandran plot	
Most favored regions	95.2
Additionally allowed regions	4.7
Generally allowed regions	0.1
Disallowed regions	0.0

[a]RDCs from the second alignment medium were used for structure validation.

[b]Statistics apply to the 10 lowest-energy structures.

[c]Pairwise r.m.s. deviation was calculated among 10 refined structures.

Extended Data Fig. 10g

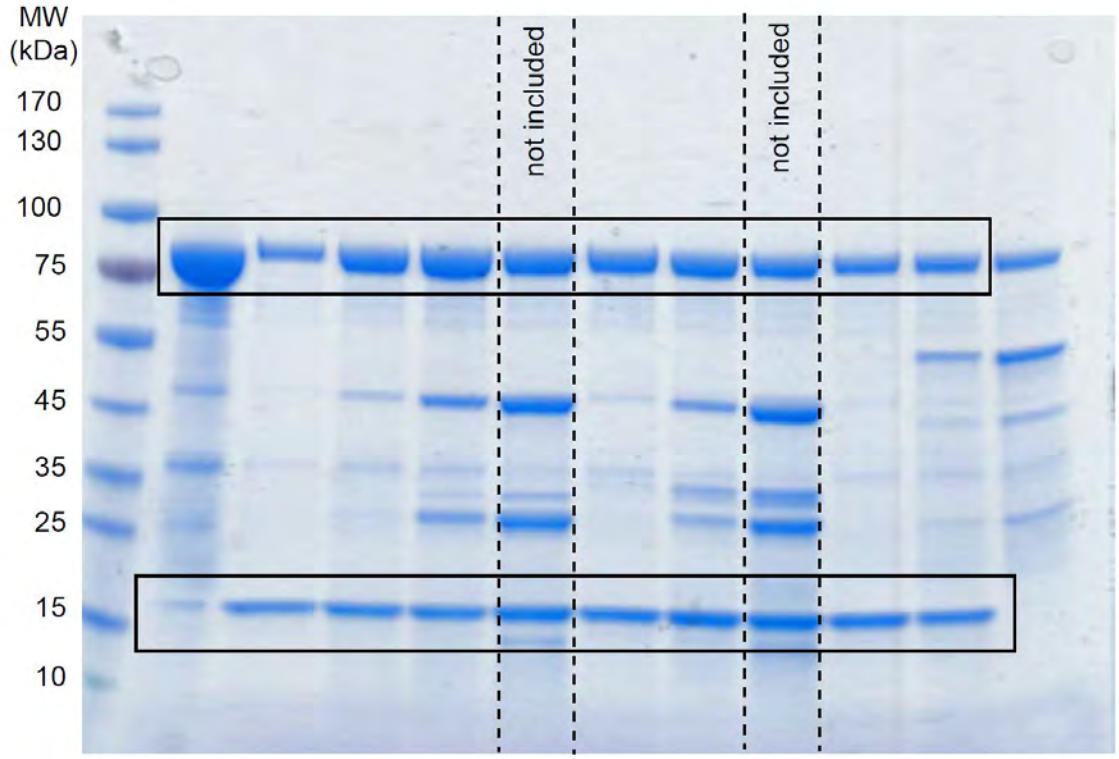

Supplementary Fig. 1 | Gel source data for Extended Data Fig. 10g. The content of Extended Data Fig. 10g is highlighted in a box. The experiment was repeated two times with similar results.